Journal of Industrial and Management Optimization

JIMO, 22(10): 5154–5193.
DOI: 10.3934/jimo.2026178
Received: 25 July 2026
Revised: 31 August 2026
Accepted: 04 September 2026
Published: 20 September 2026

https://www.aimspress.com/journal/jimo

Research article

Reliability and availability analysis of a bamboo plywood manufacturing system using a continuous-time Markov state-space model

Suresh Kumar Sahani[1,2,*], Tsair-Fwu Lee[1], Digvijay Pandey[1], Binay Kumar Pandey[1] and Kameshwar Sahani[3]

[1] Department of Electronics Engineering, National Kaohsiung University of Science and Technology, Taiwan
[2] Faculty of Science Technology and Engineering, Rajarshi Janak University, Janakpurdham, Nepal
[3] Department of Civil Engineering, Kathmandu University, Dhulikhel, Nepal

* **Correspondence:** Email: sureshsahani@rju.edu.np.

S1. Scope, contents, and how to use this document

This document consolidates, in a single self-contained file, the complete set of supplementary materials supporting the article “Reliability and Availability Analysis of a Bamboo Plywood Manufacturing System Using a Continuous-Time Markov State-Space Model” by Sahani, Lee, Pandey, Pandey, and Sahani. The parent study formulates a 34-state continuous-time Markov chain (CTMC) covering a nine-subsystem bamboo plywood production line, validates the exponential failure and repair assumptions against 26 months of plant operational logs through Anderson–Darling goodness-of-fit testing, solves the transient behaviour with a fourth-order Runge–Kutta integrator over a 360-day horizon, derives the long-run availability from the steady-state balance equations, and attaches bootstrap confidence intervals, Birnbaum importance measures, and a downtime-cost conversion model to every headline figure. The present file gathers every extension of that material that a reviewer, replicator, or plant engineer may require: full methodological protocols, the complete mathematical formulation, every data table underlying the figures and claims of the main text, all figures at reproduction quality, and an independent numerical verification of the principal results.

The organisation follows the conventions of journal supplementary materials. All tables are numbered sequentially with the prefix “S” (Table S1 through Table S26), all figures with the prefix

“S” (Figure S1 through Figure S9), and all display equations with the prefix “S” in parentheses, equation. (S1) through equation (S121). Tables S1–S5 and S10–S24 consolidate the reference tables of the main text so that this file can be read without the article at hand; Tables S6–S9, S25, and S26 are new to this compilation and report verification computations, a complete notation glossary, and a cross-reference map linking each supplementary item to the section of the main text it supports. Equations (S1)–(S36) reproduce the transient formulation; equations (S37)–(S100) reproduce the steady-state system and its recursive solution; equations (S101)–(S112) re-derive the composite-state ratios G1, G2, G3 step by step; and equations (S113)–(S121) state the importance-measure and downtime-cost formulas.

Readers who wish only to check a specific claim should begin with the cross-reference map in Section S15, which lists every quantitative statement of the main text together with the supplementary table that contains its underlying values. Readers attempting a full replication should proceed sequentially: the data-collection and screening protocol of Section S2 defines the exact sample on which all rate estimates rest, Sections S3 and S4 define the validated parameters, Section S5 contains the equation system to be implemented, and Section S6 reports an independent re-solve of that system whose outputs (the G ratios, the steady-state distribution, the availability figure, and the downtime-cost projections) agree with the published values to the precision reported in the main text. All rates are expressed per day unless stated otherwise, monetary figures are in United States dollars, and the observation window is January 2022 through February 2024.

S2. Extended materials and methods

S2.1. Cooperating plant and production sequence

The cooperating plant operates a single sequential production line with an average daily output of approximately 18 m^3 of finished bamboo plywood panel and a nominal annual capacity of approximately 6,200 m^3. The line integrates mechanical, hydrothermal, hydraulic, and finishing operations that transform bamboo culms and fast-growing wood logs into finished panels. Modern bamboo plywood production combines bamboo face veneers with a wooden core through six stages. First, core veneer production: logs of fast-growing species such as poplar (Populus spp.) or eucalyptus (Eucalyptus spp., locally known as safeda) are debarked and peeled into continuous core veneers on a rotary peeling machine, then dried to the target moisture content in a deck dryer. Second, bamboo strip preparation: bamboo culms are cross-cut, split, and processed into strips or slats, which are softened in a steaming chamber, then peeled or sliced into thin bamboo veneers, dried, and graded. Third, assembly preparation: dried bamboo strips and veneers are cut to precise dimensions on rip saws and planed to uniform thickness. Fourth, glue application: adhesive is applied uniformly to both faces of the dried core veneers with a four-roller glue spreader. Fifth, lay-up and hot pressing: bamboo veneers are laid perpendicularly or parallel on both sides of the glued core and hot-pressed under controlled temperature and pressure to cure the adhesive. Sixth, finishing: cured panels are trimmed to final dimensions on a cutting saw and surface-sanded for a smooth, uniform finish. Figure S1 shows the plant flow diagram and Figures S2–S4 show schematic cross-sections of the band saw, planer, and glue spreader, respectively.

Equipment service ages at the start of the data-collection window ranged from 3 years (sanding machine) to 11 years (peeling machine), so the fleet mixes units in early, mid, and late service life. The line operates a three-shift, 333-day schedule, corresponding to T = 8,000 operating hours per year in the downtime-cost model of Section S10. Continuous operation of every unit is necessary to maintain production flow, dimensional accuracy, and bonding quality, which is why subsystem failures propagate downstream through off-specification intermediate stock and lost throughput rather than remaining locally contained.

S2.2. Data collection and screening protocol

Daily operational logs covering January 2022 through February 2024 (26 months) were made available for the study. Each log entry records the subsystem identity, failure timestamp, repair start, repair completion, free-text failure-mode description, and the maintenance action taken. In total, 1,134 failure events were extracted across the nine subsystems, with subsystem-level event counts ranging from 41 (cutting saw) to 218 (steaming chamber). Before rate estimation, the raw extraction was screened with three explicit rules: (i) duplicate entries, identified by identical subsystem, failure timestamp, and repair-completion timestamp, were removed; (ii) entries with ambiguous timestamps, meaning log rows in which the failure time, repair start, or repair completion could not be resolved to a unique calendar time, were excluded; and (iii) events without documented repair completion, meaning failures recorded during the final days of the observation window whose repair fell outside it, were excluded to avoid right-censoring bias in the repair-time distribution. Application of these rules removed 27 entries, leaving 1,107 events for rate estimation. Inter-failure times were computed as the difference between successive failure timestamps of the same subsystem, and repair durations as the difference between repair completion and repair start. All rates in this document are expressed in failures or repairs per day and estimated by maximum likelihood as reciprocals of the corresponding sample means.

S2.3. Subsystem inventory and failure modes

Table S1 summarises the nine repairable subsystems, their principal mechanical, thermal, and hydraulic components, dominant failure modes, and standby arrangements. Five of the nine subsystems carry spare parts (spare belt for the band saw, spare cutters for the rip saw and cutting saw, spare blades for the planer, spare belt for the sanding machine), which motivates the instantaneous-and-perfect standby switching assumption (vii) of Section S2.7. The steaming chamber and dryer are the only two multi-motor units whose single-component failures produce a measurable but partial throughput reduction, which is the physical basis for their three-state (full, reduced, failed) representation.

Table S1. Inventory of the nine repairable subsystems of the bamboo plywood manufacturing line, their key components, dominant failure modes, and standby arrangements (consolidates Table 1 of the main text).

Subsystem	Designation	Main function	Key components	Failure modes	Standby
R_1	Band Saw	Cuts logs into strips	Motor, blade, belt	Full failure	Spare belt
R_2	Steaming Chamber	Softens / conditions woodpieces	3 motors, 3 fans	Reduced (single), Full (multiple)	None
R_3	Rip Saw	Precision cutting of components	Motor, roller, 7 diamond cutters	Primarily full	Spare cutters
R_4	Planer	Uniform thickness planing	Motor, 4 blades, feed rollers	Full failure	Spare blades
R_5	Peeling Machine	Produces core veneers	Motor, 6 bearings, roller, gearbox	Full failure only	None
R_6	Dryer	Dries core veneers	5 motors, 4 fans, hydraulic pump	Reduced (single), Full (multiple)	None
R_7	Hot Press	Bonds layers under heat and pressure	2 motors, 8 cylinders, thermo-oil pump, control panel	Full failure only	None
R_8	Cutting Saw	Cuts panels to final size	2 motors, 2 diamond cutters	Primarily full	Spare cutters
R_9	Sanding Machine	Surface finishing	Motor, sanding belt, extraction fan	Full failure	Spare belt

*Note: Failure-mode descriptors follow the plant maintenance vocabulary. “Reduced (single), Full (multiple)” denotes partial-capacity operation after a single motor or fan failure and complete stoppage after multi-fault conditions.

S2.4. Notation convention

Each subsystem Ri (i = 1, …, 9) carries the failure rate λi and the repair rate μi with the same index. The two additional transition rates required for the reduced-capacity structure of the steaming chamber (R2) and the dryer (R6) are denoted λ10 and λ11, and their directions are stated explicitly to avoid ambiguity: λ10 is the transition rate from the reduced-capacity state of the steaming chamber (r2′) to its fully failed state (r2), and λ11 is the transition rate from the reduced-capacity state of the dryer (r6′) to its fully failed state (r6). Repair rates μ10 and μ11 are not required because repair from any failed or reduced-capacity state is assumed to restore the subsystem directly to full capacity. Within the model equations, λ8 denotes the full-to-reduced degradation rate of R2 and λ9 the full-to-reduced degradation rate of R6, as summarised in Table S5. This convention is applied uniformly in every equation, table, figure legend, and in-text reference of the main text and of this document; the complete symbol glossary is given in Table S25.

S2.5. Failure-mode and effects analysis (FMEA) and state-aggregation protocol

Table S2. Failure-mode and effects analysis (FMEA) with risk priority numbers (RPN) justifying the binary versus three-state modelling choice for each subsystem (consolidates Table 2 of the main text).

Subsystem	Dominant failure mode	Effect	S	O	D	RPN	State model
R_1 Band Saw	Blade breakage / belt slippage / bearing seizure	Line stoppage until blade replaced	7	4	6	168	Binary (bimodal)
R_2 Steaming Chamber	Single motor / fan failure → reduced throughput; multiple → full stop	Degraded heating; line slowdown; full stoppage at multi-fault	8	6	5	240	Three-state
R_3 Rip Saw	Cutter chipping / motor overload / feed roller wear	Cut quality loss; line stoppage	6	3	5	90	Binary
R_4 Planer	Blade wear / motor failure / bearing seizure	Thickness non-uniformity; line stoppage	6	3	5	90	Binary
R_5 Peeling Machine	Gearbox failure / bearing seizure / motor overload	Veneer supply interruption; line stoppage	9	4	7	252	Binary
R_6 Dryer	Single motor / fan failure → reduced drying; multiple → full stop	Moisture non-uniformity; full stoppage at multi-fault	8	5	5	200	Three-state
R_7 Hot Press	Hydraulic leakage / thermo-oil pump failure / heating fault	Bonding failure; panel scrap; line stoppage	9	3	6	162	Binary
R_8 Cutting Saw	Cutter breakage / motor overload / alignment drift	Off-spec panel; line stoppage	5	3	6	90	Binary
R_9 Sanding Machine	Belt tearing / motor failure / bearing seizure	Surface roughness; line stoppage	5	3	6	90	Binary

*Note: S = severity, O = occurrence, D = detectability, each on a 1–10 scale; RPN = S × O × D. Subsystems with RPN ≤ 125 and bimodal dwell behaviour were modelled as binary; the steaming chamber and dryer carry an additional reduced-capacity state.

To justify the choice of a binary versus a three-state representation for each subsystem, a formal failure-mode and effects analysis was conducted using the plant operational logs and structured interviews with the maintenance supervisor. Each dominant failure mode was scored on severity (S, 1–10), occurrence (O, 1–10), and detectability (D, 1–10), and the risk priority number RPN = S × O × D was computed. Subsystems whose dominant failure modes had RPN ≤ 125 and exhibited sharply bimodal behaviour, meaning the unit was either fully operational or fully failed with negligible intermediate dwell time, were modelled as binary. Subsystems with non-negligible intermediate-state dwell time, specifically the steaming chamber and the dryer, both of which contain multiple motors and circulation fans whose individual failure produces a measurable but partial throughput reduction, were modelled with an additional reduced-capacity state. Table S2 reports the full FMEA scoring together with the resulting state-model choice per subsystem.

S2.6. Complete enumeration of the 34 system states

For full reproducibility, all 34 states of the CTMC are enumerated in Table S3. State indices follow the order: full-capacity composite states first (1–4), then single-subsystem-failure states (5–11), then failed-plus-reduced states for the steaming-chamber branch (12–18), the dryer branch (19–25), and the both-reduced branch (26–32), and finally the two consolidated reduced-to-failed states (33–34). The aggregation protocol collapses the combinatorial space of subsystem-status combinations into the 34 states that carry non-negligible probability mass under the plant's observed failure intensities; combinations involving simultaneous failure of three or more subsystems were merged into the corresponding two-failure states because their steady-state probabilities are below 10-6 under the validated rate ranges. The system transition diagram is reproduced as Figure S5.

Table S3. Complete enumeration of the 34 states in the CTMC model (consolidates Table 3 of the main text).

State	Definition
1	All nine subsystems at full capacity.
2	R_2 in reduced-capacity state r_2'; all others at full capacity.
3	R_6 in reduced-capacity state r_6'; all others at full capacity.
4	R_2 and R_6 both in reduced-capacity states; all others at full capacity.
5	R_1 failed (r_1); all others at full capacity.
6	R_2 failed (r_2); all others at full capacity.
7	R_3 failed (r_3); all others at full capacity.
8	R_4 failed (r_4); all others at full capacity.
9	R_5 failed (r_5); all others at full capacity.
10	R_6 failed (r_6); all others at full capacity.
11	R_7 failed (r_7); all others at full capacity.
12	R_1 failed + R_2 reduced (r_1, r_2').

Continued on next page

State	Definition
13	R_2 failed + R_1 failed (r_2, r_1).
14	R_3 failed + R_2 reduced (r_3, r_2').
15	R_4 failed + R_2 reduced (r_4, r_2').
16	R_5 failed + R_2 reduced (r_5, r_2').
17	R_6 failed + R_2 reduced (r_6, r_2').
18	R_7 failed + R_2 reduced (r_7, r_2').
19	R_1 failed + R_6 reduced (r_1, r_6').
20	R_2 failed + R_6 reduced (r_2, r_6').
21	R_3 failed + R_6 reduced (r_3, r_6').
22	R_4 failed + R_6 reduced (r_4, r_6').
23	R_5 failed + R_6 reduced (r_5, r_6').
24	R_7 failed + R_6 reduced (r_7, r_6').
25	R_1 failed + both R_2 and R_6 reduced (r_1, r_2', r_6').
26	R_2 failed + both reduced (r_2, r_6').
27	R_3 failed + both reduced (r_3, r_2', r_6').
28	R_4 failed + both reduced (r_4, r_2', r_6').
29	R_5 failed + both reduced (r_5, r_2', r_6').
30	R_6 failed + both reduced (r_6, r_2').
31	R_7 failed + both reduced (r_7, r_2', r_6').
32	R_8 failed + both reduced (r_8, r_2', r_6').
33	Steaming chamber in failed state r_2 reached from reduced state r_2' (consolidated).
34	Dryer in failed state r_6 reached from reduced state r_6' (consolidated).

*Note: The glue spreader is assumed failure-free (assumption ii, Section S2.7) and therefore does not appear as a modelled failure state. Combinations of three or more simultaneous subsystem failures are merged into the corresponding two-failure states because their steady-state probabilities fall below 10^{-6}.

S2.7. Model assumptions

The CTMC formulation rests on seven explicit assumptions, reproduced here verbatim in substance from the main text so that the model boundaries are unambiguous for any replication attempt:

(ii) Failure and repair times are assumed to be exponentially distributed with constant rates, independent of time and of each other. All rates are expressed in failures or repairs per day. This assumption is empirically validated in Section S3.

(iii) The glue spreader, considered an integral part of the production line, has an extremely low failure rate and is assumed to be failure-free for the purpose of this model.

(iiii) No common-cause failures or cascading failures occur between subsystems. Plant records indicate that common-cause events contributed fewer than 3% of historical failures, supporting this assumption for the cooperating facility.

(iiv) Only subsystems R2 (steaming chamber) and R6 (dryer) are modelled with an intermediate reduced-capacity state; all other subsystems have only two states, full capacity or complete failure. The justification is given by the FMEA of Section S2.5.

(iv) Repair of a subsystem in the reduced-capacity state (R2 or R6) restores it to the full-capacity state; no partial repair outcomes are considered.

(ivi) Repaired components are assumed to be "as good as new", meaning repair restores the component to a condition statistically identical to a new one.

(ivii) Switching to standby components (where available) is instantaneous and perfect, with no switching time and no failure during switchover.

S3. Distributional validation of the markovian assumption

S3.1. Estimation and testing methodology

The exponential-distribution assumption was tested empirically before model construction, treating the memoryless hypothesis as a testable proposition rather than a modelling convenience. For each subsystem, inter-failure times and repair durations were extracted from the screened operational logs of Section S2.2. The rate parameters were obtained by maximum likelihood, $\lambda i = 1$ / (sample mean of inter-failure times) for failures and $\mu i = 1$ / (sample mean of repair durations) for repairs. The Anderson–Darling statistic A2 was then computed against the exponential null hypothesis for each sample. The Anderson–Darling test gives greater weight to the tails of the distribution than the Kolmogorov–Smirnov test and is therefore the more appropriate choice for detecting the heavy right tail that would indicate ageing or wear-out behaviour. The 5% critical value for the fully specified exponential case is A2crit = 1.328; samples with A2 below 1.328 are classified "Accept", samples with $1.328 \leq A2 < 2.0$ are classified "Marginal", and samples with $A2 \geq 1.328$ and $p < 0.05$ are classified "Reject".

S3.2. Complete goodness-of-fit results

Table S4 reports the test statistics for all eleven failure processes (nine subsystem failure or degradation processes plus the two reduced-to-failed transition processes) and all nine repair processes. Nine of the eleven failure processes and eight of the nine repair processes pass the Anderson–Darling test at the 5% significance level, providing empirical support for the Markovian assumption underlying the CTMC formulation.

Table S4. Anderson–Darling goodness-of-fit test against the exponential distribution for inter-failure and repair-time samples of every subsystem (consolidates Table 4 of the main text). Critical value at 5% significance: A2crit = 1.328. “Marginal” denotes $1.328 \leq A2 < 2.0$; “Reject” denotes $A2 \geq 1.328$ with $p < 0.05$.

Subsystem	n (fail)	λ (per day)	A^2	Exp.?	n (rep)	μ (per day)	A^2	Exp.?
R_1 Band Saw	137	$\lambda_1 = 0.0027$	0.842	Accept	0.67	$\mu_1 = 0.67$	0.711	Accept
R_2 Steaming Chamber	218	$\lambda_2 = 0.0018$	0.921	Accept	0.83	$\mu_2 = 0.83$	0.694	Accept
R_3 Rip Saw	92	$\lambda_3 = 0.0018$	1.118	Accept	0.83	$\mu_3 = 0.83$	0.836	Accept
R_4 Planer	78	$\lambda_4 = 0.0027$	1.241	Accept	0.67	$\mu_4 = 0.67$	0.887	Accept
R_5 Peeling Machine	163	$\lambda_5 = 0.0102$	1.498	Marginal	10.20	$\mu_5 = 10.20$	0.612	Accept
R_6 Dryer	141	$\lambda_6 = 0.0027$	0.884	Accept	0.67	$\mu_6 = 0.67$	0.728	Accept
R_7 Hot Press	108	$\lambda_7 = 0.0027$	0.952	Accept	0.67	$\mu_7 = 0.67$	0.782	Accept
R_8 Cutting Saw	41	$\lambda_8 = 0.017$	1.882	Reject	0.67	$\mu_8 = 0.934$	Accept	
R_9 Sanding Machine	66	$\lambda_9 = 0.0027$	1.067	Accept	0.50	$\mu_9 = 0.711$	Accept	
R_2 reduced → failed	47	$\lambda_{10} = 0.0055$	0.812	Accept	—	—	—	—
R_6 reduced → failed	29	$\lambda_{11} = 0.00054$	0.774	Accept	—	—	—	—

*Note: n (fail) and n (rep) are the screened sample sizes for inter-failure and repair-time samples respectively; values are transcribed as printed in the main text. The two reduced-to-failed processes have no separate repair samples because repair from any failed state restores full capacity directly.

S3.3. Treatment of the marginal and rejected cases

Two failure processes depart from strict exponentiality and warrant comment. The peeling-machine failure distribution is marginal (A2 = 1.498); a supplementary Weibull fit gave a shape parameter $k = 1.08$, very close to the exponential case $k = 1$, so the exponential was retained for model uniformity. The cutting-saw failure distribution formally rejects the exponential null (A2 = 1.882); however, given the small sample size ($n = 41$) and the cutting-saw’s low criticality ranking (Section S9), the resulting model error is bounded and the exponential was retained subject to the sensitivity analysis of Section S7. For these two subsystems, a semi-Markov extension with Weibull or lognormal sojourn-time distributions would more faithfully capture the underlying degradation physics at the cost of analytical tractability, and is identified in the main text as a direction for future work. Overall, the validation provides empirical support, not merely modelling convenience, for the Markovian assumption underlying the CTMC formulation.

S4. Baseline rate estimates and sensitivity-range provenance

Table S5 reports the baseline failure and repair rates estimated from the screened operational logs under nominal operating conditions, together with the screened event counts and the implied mean time between failures per transition. These values are the central scenario for every transient and steady-state computation reported in the main text and re-verified in Section S6 of this document. The rate set distinguishes full-capacity failure rates λ1–λ7 for subsystems R1–R7, the full-to-reduced degradation rates λ8 (steaming chamber) and λ9 (dryer), and the reduced-to-failed transition rates λ10 (steaming chamber) and λ11 (dryer). Note that the cutting saw (R8) and sanding machine (R9) are primarily protected by standby spares and their failure behaviour enters the sensitivity ranges only through the FMEA ranking and the Birnbaum importance analysis of Section S9.

Table S5. Baseline transition and repair rates under nominal operating conditions, estimated from screened plant operational logs (January 2022–February 2024); consolidates Table 5 of the main text. λ1–λ7 are full-capacity failure rates for R1–R7; λ8 and λ9 are degradation rates (full → reduced) for R2 and R6 respectively; λ10 and λ11 are reduced → failed transition rates for R2 and R6.

Subsystem / transition	Rate (per day)	Repair rate (per day)	n	MTBF (days)
R_1 Band Saw	$\lambda_1 = 0.0027$	$\mu_1 = 0.67$	137	370.4
R_2 Steaming Chamber	$\lambda_2 = 0.0018$	$\mu_2 = 0.83$	218	555.6
R_3 Rip Saw	$\lambda_3 = 0.0018$	$\mu_3 = 0.83$	92	555.6
R_4 Planer	$\lambda_4 = 0.0027$	$\mu_4 = 0.67$	78	370.4
R_5 Peeling Machine	$\lambda_5 = 0.0102$	$\mu_5 = 10.20$	163	98.0
R_6 Dryer	$\lambda_6 = 0.0027$	$\mu_6 = 0.67$	141	370.4
R_7 Hot Press	$\lambda_7 = 0.0027$	$\mu_7 = 0.67$	108	370.4
R_2 full → reduced	$\lambda_8 = 0.017$	—	47	58.8
R_6 full → reduced	$\lambda_9 = 0.0027$	—	41	370.4
R_2 reduced → failed	$\lambda_{10} = 0.0055$	—	47	181.8
R_6 reduced → failed	$\lambda_{11} = 0.00054$	—	29	1851.9

*Note: MTBF entries are the reciprocals of the corresponding rates in days. n is the screened event count per transition (Section S2.2).

Provenance of the sensitivity-analysis variation ranges. Each range used in the sensitivity tables of Section S7 is constructed from the empirical 5th-to-95th percentile window of the corresponding monthly-aggregated rate estimate over the 26-month observation period. The lower bound corresponds to a month in which the subsystem exhibited its best observed reliability, typically a month following a preventive maintenance cycle, and the upper bound corresponds to a month in which a degraded operating regime was documented, for example the monsoon period for the steaming chamber, when elevated humidity increased motor-failure frequency. The ranges therefore reflect historical extremes of the cooperating plant rather than industry-typical fluctuation intervals or artificially set values. For example, λ10 ranges from 0.0041 (5th percentile, dry-season months) to 0.0083 (95th percentile, monsoon months), and λ5 ranges from 0.0067 (post-preventive-maintenance months) to 0.0113 (months with documented gearbox temperature excursions). All variation ranges used in Tables S10 through S21 are constructed in this manner.

S5. Complete mathematical formulation of the CTMC model

This section consolidates the complete equation system of the model: the 34 transient state equations, the 34 steady-state balance equations, the 30 recursive steady-state solutions, the closed-form composite-state ratios G1, G2, G3 together with their step-by-step derivation, the normalisation and availability expressions, the Birnbaum importance-measure definitions, and the downtime-cost model. Equations are transcribed from the main text and renumbered sequentially with the prefix S; the structure of the system is as follows. Equations (S1)–(S4) govern the four composite full-capacity and reduced-capacity states; equations (S5)–(S11) govern the single-subsystem failed states with all other subsystems at full capacity; equations (S12)–(S18) govern the failed-plus-reduced states of the steaming-chamber branch; equations (S19)–(S25) govern the failed-plus-reduced states of the dryer branch; equations (S26)–(S32) govern the failed-plus-both-reduced states; and equations (S33)–(S34) govern the two consolidated reduced-to-failed transitions. Two transcription conventions deserve note. First, the transient inflow terms of equation (S1) are printed in the main text with the symbols μ8f33(t) and μ9f34(t), while the corresponding steady-state and recursive relations, equations (S69) and (S70) below, apply the consolidated repair convention μ2f33 and μ6f34; both conventions are reproduced exactly as printed, and the steady-state convention is the one carried through the closed-form solution. Second, the transient equations of states 24 and 31 carry the rate λ6 as printed, whereas their steady-state counterparts (S60) and (S67) carry λ11; the recursive relations follow the steady-state convention. These transcription notes are supplied so that implementers can reproduce the published steady-state results exactly, as verified independently in Section S6.

S5.1. Transient state equations

Probability considerations give the following system of differential equations governing the CTMC, solved numerically with the Runge–Kutta specification of Section S6.1:

$$df_1(t)/dt + (\lambda_1 + \lambda_2 + \lambda_3 + \lambda_4 + \lambda_5 + \lambda_6 + \lambda_7 + \lambda_8 + \lambda_9)\, f_1(t) =$$

$$\mu_1 f_5(t) + \mu_2 f_6(t) + \mu_3 f_7(t) + \mu_4 f_8(t) + \mu_5 f_9(t) + \mu_6 f_{10}(t) + \mu_7 f_{11}(t) + \mu_8 f_{33}(t) + \mu_9 f_{34}(t) \quad \text{(S1)}$$

$$df_2(t)/dt + (\lambda_1 + \lambda_2 + \lambda_3 + \lambda_4 + \lambda_6 + \lambda_7 + \lambda_9 + \lambda_{10})\, f_2(t) =$$

$$\mu_1 f_{12}(t) + \mu_2 f_{13}(t) + \mu_3 f_{14}(t) + \mu_4 f_{15}(t) + \mu_5 f_{16}(t) + \mu_6 f_{17}(t) + \mu_7 f_{18}(t) \quad \text{(S2)}$$

$$df_3(t)/dt + (\lambda_1 + \lambda_2 + \lambda_3 + \lambda_4 + \lambda_5 + \lambda_6 + \lambda_7 + \lambda_8 + \lambda_{11})\, f_3(t) =$$

$$\mu_1 f_{19}(t) + \mu_2 f_{20}(t) + \mu_3 f_{21}(t) + \mu_4 f_{22}(t) + \mu_5 f_{23}(t) + \mu_6 f_{24}(t) \quad \text{(S3)}$$

$$df_4(t)/dt + (\lambda_1 + \lambda_2 + \lambda_3 + \lambda_4 + \lambda_5 + \lambda_6 + \lambda_7 + \lambda_{10} + \lambda_{11})\, f_4(t) =$$

$$\mu_1 f_{26}(t) + \mu_2 f_{27}(t) + \mu_3 f_{28}(t) + \mu_4 f_{29}(t) + \lambda_5 f_3(t) + \lambda_6 f_2(t) \quad \text{(S4)}$$

$$df_5(t)/dt + \mu_1 f_5(t) = \lambda_1 f_1(t) \quad \text{(S5)}$$

$$df_6(t)/dt + \mu_2 f_6(t) = \lambda_2 f_1(t) \quad \text{(S6)}$$

$$df_7(t)/dt + \mu_3 f_7(t) = \lambda_3 f_1(t) \quad \text{(S7)}$$

$$df_8(t)/dt + \mu_4 f_8(t) = \lambda_4 f_1(t) \quad \text{(S8)}$$

$$df_9(t)/dt + \mu_5 f_9(t) = \lambda_5 f_1(t) \tag{S9}$$

$$df_{10}(t)/dt + \mu_6 f_{10}(t) = \lambda_6 f_1(t) \tag{S10}$$

$$df_{11}(t)/dt + \mu_7 f_{11}(t) = \lambda_7 f_1(t) \tag{S11}$$

$$df_{12}(t)/dt + \mu_1 f_{12}(t) = \lambda_1 f_2(t) \tag{S12}$$

$$df_{13}(t)/dt + \mu_2 f_{13}(t) = \lambda_{10} f_2(t) \tag{S13}$$

$$df_{14}(t)/dt + \mu_3 f_{14}(t) = \lambda_3 f_2(t) \tag{S14}$$

$$df_{15}(t)/dt + \mu_4 f_{15}(t) = \lambda_4 f_2(t) \tag{S15}$$

$$df_{16}(t)/dt + \mu_5 f_{16}(t) = \lambda_5 f_2(t) \tag{S16}$$

$$df_{17}(t)/dt + \mu_6 f_{17}(t) = \lambda_6 f_2(t) \tag{S17}$$

$$df_{18}(t)/dt + \mu_7 f_{18}(t) = \lambda_7 f_2(t) \tag{S18}$$

$$df_{19}(t)/dt + \mu_1 f_{19}(t) = \lambda_1 f_3(t) \tag{S19}$$

$$df_{20}(t)/dt + \mu_2 f_{20}(t) = \lambda_2 f_3(t) \tag{S20}$$

$$df_{21}(t)/dt + \mu_3 f_{21}(t) = \lambda_3 f_3(t) \tag{S21}$$

$$df_{22}(t)/dt + \mu_4 f_{22}(t) = \lambda_4 f_3(t) \tag{S22}$$

$$df_{23}(t)/dt + \mu_5 f_{23}(t) = \lambda_5 f_3(t) \tag{S23}$$

$$df_{24}(t)/dt + \mu_6 f_{24}(t) = \lambda_6 f_3(t) \tag{S24}$$

$$df_{25}(t)/dt + \mu_7 f_{25}(t) = \lambda_7 f_3(t) \tag{S25}$$

$$df_{26}(t)/dt + \mu_1 f_{26}(t) = \lambda_1 f_4(t) \tag{S26}$$

$$df_{27}(t)/dt + \mu_2 f_{27}(t) = \lambda_2 f_4(t) \tag{S27}$$

$$df_{28}(t)/dt + \mu_3 f_{28}(t) = \lambda_3 f_4(t) \tag{S28}$$

$$df_{29}(t)/dt + \mu_4 f_{29}(t) = \lambda_4 f_4(t) \tag{S29}$$

$$df_{30}(t)/dt + \mu_5 f_{30}(t) = \lambda_5 f_4(t) \tag{S30}$$

$$df_{31}(t)/dt + \mu_6 f_{31}(t) = \lambda_6 f_4(t) \tag{S31}$$

$$df_{32}(t)/dt + \mu_7 f_{32}(t) = \lambda_7 f_4(t) \tag{S32}$$

$$df_{33}(t)/dt + \mu_2 f_{33}(t) = \lambda_{10} f_2(t) + \lambda_{10} f_4(t) \tag{S33}$$

$$df_{34}(t)/dt + \mu_6 f_{34}(t) = \lambda_{11} f_3(t) + \lambda_{11} f_4(t) \tag{S34}$$

$$f_1(0) = 1,\ f_r(0) = 0 \text{ for } r = 2, 3, \ldots, 34 \tag{S35}$$

$$R(t) = f_1(t) + f_2(t) + f_3(t) + f_4(t) \tag{S36}$$

The initial condition vector corresponds to a freshly commissioned line, and system reliability R(t) is the probability of residing in one of the four composite up-states, the states in which no subsystem is fully failed. It should be noted that in this numerical analysis only the primary subsystems are taken into account and certain value combinations are not all-inclusive; the system's dependability is calculated using various combinations of failure and repair rates as detailed in Sections S7 and S8.

S5.2. Steady-state balance equations

The long-run behaviour of the system is obtained by setting the time derivatives in equations (S1)–(S34) to zero and accounting for the steady-state constraints, which gives the following algebraic balance equations:

$$(\lambda 1 + \lambda 2 + \lambda 3 + \lambda 4 + \lambda 5 + \lambda 6 + \lambda 7 + \lambda 8 + \lambda 9)\, f1 =$$

$$\mu 1f5 + \mu 2f6 + \mu 3f7 + \mu 4f8 + \mu 5f9 + \mu 6f10 + \mu 7f11 + \mu 2f33 + \mu 6f34 \tag{S37}$$

$$(\lambda_1 + \lambda_3 + \lambda_4 + \lambda_5 + \lambda_6 + \lambda_7 + \lambda_9 + \lambda_{10})\, f_2 =$$

$$\mu_1 f_{12} + \mu_2 f_{13} + \mu_3 f_{14} + \mu_4 f_{15} + \mu_5 f_{16} + \mu_6 f_{17} + \mu_7 f_{18} + \lambda_8 f_1 \tag{S38}$$

$$(\lambda_1 + \lambda_2 + \lambda_3 + \lambda_4 + \lambda_5 + \lambda_6 + \lambda_7 + \lambda_8 + \lambda_{11})\, f_3 =$$

$$\mu_1 f_{19} + \mu_2 f_{20} + \mu_3 f_{21} + \mu_4 f_{22} + \mu_5 f_{23} + \mu_6 f_{24} + \mu_7 f_{25} + \lambda_9 f_1 \tag{S39}$$

$$(\lambda_1 + \lambda_2 + \lambda_3 + \lambda_4 + \lambda_5 + \lambda_6 + \lambda_7 + \lambda_{10} + \lambda_{11})\, f_4 =$$

$$\mu_1 f_{26} + \mu_2 f_{27} + \mu_3 f_{28} + \mu_4 f_{29} + \mu_5 f_{30} + \mu_6 f_{31} + \mu_7 f_{32} + \lambda_8 f_3 + \lambda_9 f_2 \tag{S40}$$

$$\mu_1 f_5 = \lambda_1 f_1 \tag{S41}$$

$$\mu_2 f_6 = \lambda_2 f_1 \tag{S42}$$

$$\mu_3 f_7 = \lambda_3 f_1 \tag{S43}$$

$$\mu_4 f_8 = \lambda_4 f_1 \tag{S44}$$

$$\mu_5 f_9 = \lambda_5 f_1 \tag{S45}$$

$$\mu_6 f_{10} = \lambda_6 f_1 \tag{S46}$$

$$\mu_7 f_{11} = \lambda_7 f_1 \tag{S47}$$

$$\mu_1 f_{12} = \lambda_1 f_2 \tag{S48}$$

$$\mu_2 f_{13} = \lambda_{10} f_2 \tag{S49}$$

$$\mu_3 f_{14} = \lambda_3 f_2 \tag{S50}$$

$$\mu_4 f_{15} = \lambda_4 f_2 \tag{S51}$$

$$\mu_5 f_{16} = \lambda_5 f_2 \tag{S52}$$

$$\mu_6 f_{17} = \lambda_6 f_2 \tag{S53}$$

$$\mu_7 f_{18} = \lambda_7 f_2 \tag{S54}$$

$$\mu_1 f_{19} = \lambda_1 f_3 \tag{S55}$$

$$\mu_2 f_{20} = \lambda_2 f_3 \tag{S56}$$

$$\mu_3 f_{21} = \lambda_3 f_3 \tag{S57}$$

$$\mu_4 f_{22} = \lambda_4 f_3 \quad (S58)$$

$$\mu_5 f_{23} = \lambda_5 f_3 \quad (S59)$$

$$\mu_6 f_{24} = \lambda_{11} f_3 \quad (S60)$$

$$\mu_7 f_{25} = \lambda_7 f_3 \quad (S61)$$

$$\mu_1 f_{26} = \lambda_1 f_4 \quad (S62)$$

$$\mu_2 f_{27} = \lambda_2 f_4 \quad (S63)$$

$$\mu_3 f_{28} = \lambda_3 f_4 \quad (S64)$$

$$\mu_4 f_{29} = \lambda_4 f_4 \quad (S65)$$

$$\mu_5 f_{30} = \lambda_5 f_4 \quad (S66)$$

$$\mu_6 f_{31} = \lambda_{11} f_4 \quad (S67)$$

$$\mu_7 f_{32} = \lambda_7 f_4 \quad (S68)$$

$$\mu_2 f_{33} = \lambda_{10} f_2 + \lambda_{10} f_4 \quad (S69)$$

$$\mu_6 f_{34} = \lambda_{11} f_3 + \lambda_{11} f_4 \quad (S70)$$

S5.3. Recursive steady-state solutions, composite ratios, and availability

Solving the balance equations recursively yields the following explicit expressions for the state probabilities in terms of f1, f2, f3, f4:

$$f_5 = (\lambda_1 / \mu_1)\, f_1 \quad (S71)$$

$$f_6 = (\lambda_2 / \mu_2)\, f_1 \quad (S72)$$

$$f_7 = (\lambda_3 / \mu_3)\, f_1 \quad (S73)$$

$$f_8 = (\lambda_4 / \mu_4)\, f_1 \quad (S74)$$

$$f_9 = (\lambda_5 / \mu_5)\, f_1 \quad (S75)$$

$$f_{10} = (\lambda_6 / \mu_6)\, f_1 \quad (S76)$$

$$f_{11} = (\lambda_7 / \mu_7)\, f_1 \quad (S77)$$

$$f_{12} = (\lambda_1 / \mu_1)\, f_2 \quad (S78)$$

$$f_{13} = (\lambda_{10} / \mu_2)\, f_2 \quad (S79)$$

$$f_{14} = (\lambda_3 / \mu_3)\, f_2 \quad (S80)$$

$$f_{15} = (\lambda_4 / \mu_4)\, f_2 \quad (S81)$$

$$f_{16} = (\lambda_5 / \mu_5)\, f_2 \quad (S82)$$

$$f_{17} = (\lambda_6 / \mu_6)\, f_2 \quad (S83)$$

$$f_{18} = (\lambda_7 / \mu_7)\, f_2 \quad (S84)$$

$$f_{19} = (\lambda_1 / \mu_1)\, f_3 \tag{S85}$$

$$f_{20} = (\lambda_2 / \mu_2)\, f_3 \tag{S86}$$

$$f_{21} = (\lambda_3 / \mu_3)\, f_3 \tag{S87}$$

$$f_{22} = (\lambda_4 / \mu_4)\, f_3 \tag{S88}$$

$$f_{23} = (\lambda_5 / \mu_5)\, f_3 \tag{S89}$$

$$f_{24} = (\lambda_{11} / \mu_6)\, f_3 \tag{S90}$$

$$f_{25} = (\lambda_7 / \mu_7)\, f_3 \tag{S91}$$

$$f_{26} = (\lambda_1 / \mu_1)\, f_4 \tag{S92}$$

$$f_{27} = (\lambda_2 / \mu_2)\, f_4 \tag{S93}$$

$$f_{28} = (\lambda_3 / \mu_3)\, f_4 \tag{S94}$$

$$f_{29} = (\lambda_4 / \mu_4)\, f_4 \tag{S95}$$

$$f_{30} = (\lambda_5 / \mu_5)\, f_4 \tag{S96}$$

$$f_{31} = (\lambda_{11} / \mu_6)\, f_4 \tag{S97}$$

$$f_{32} = (\lambda_7 / \mu_7)\, f_4 \tag{S98}$$

$$f_{33} = (\lambda_{10} / \mu_2)\, f_2 + (\lambda_{10} / \mu_2)\, f_4 \tag{S99}$$

$$f_{34} = (\lambda_{11} / \mu_6)\, f_3 + (\lambda_{11} / \mu_6)\, f_4 \tag{S100}$$

The four composite up-states are linked to one another by three ratios G1, G2, G3, whose step-by-step derivation is given in Section S5.4:

$$f_2 = G_1 f_1, \; where \;\; G_1 = \frac{\lambda_8}{\lambda_9 + \lambda_{10}} \tag{S101}$$

$$f_3 = G_2 f_1, \; where \;\; G_2 = \frac{\lambda_9}{\lambda_8 + \lambda_{11}} \tag{S102}$$

$$f_4 = G_3 f_1, \; where \;\; G_3 = \frac{\lambda_8 G_2 + \lambda_9 G_1}{\lambda_{10} + \lambda_{11}} \tag{S103}$$

$$f_1 + f_2 + f_3 + f_4 + f_5 + \ldots + f_{33} + f_{34} = 1 \tag{S104}$$

$$f_1 = \{[1 + G_1 + G_2 + G_3]\,[1 + \lambda_1/\mu_1 + \lambda_2/\mu_2 + \lambda_3/\mu_3 + \lambda_4/\mu_4 + \lambda_5/\mu_5 + \lambda_6/\mu_6 + \lambda_7/\mu_7] + (\lambda_{10}/\mu_2)(G_1 + G_3) + (\lambda_{11}/\mu_6)(G_2 + G_3)\}^{-1} \tag{S105}$$

$$A(\infty) = f_1 + f_2 + f_3 + f_4 = (1 + G_1 + G_2 + G_3)\, f_1 \tag{S106}$$

Equation (S105) is the closed-form normalisation printed in the main text; it aggregates the seven single-failure ratios $\lambda i / \mu i$ uniformly across the four composite branches. The exact normalisation of the recursive relations above replaces the single bracketed sum by the three branch-specific sums (states 12–18, 19–25, and 26–32 respectively) evaluated with their branch-specific rate ratios; the difference between the two normalisations is below 0.1% under the baseline rate set, and both are evaluated numerically in Section S6.3. The long-run availability $A(\infty)$ is the steady-state probability that the line resides in one of the four composite up-states, equation (S106). With the baseline rate set the numerical values are G1 ≈ 2.073, G2 ≈ 0.154, G3 ≈ 1.360, f1 ≈ 0.212, and A(∞) ≈ 0.973, as derived step by step in the next subsection and verified independently in Section S6.

S5.4. Step-by-step derivation of the ratios G_{1}, G_{2}, G_{3}

Step 1, derivation of G1. Consider the steady-state balance for the reduced-capacity composite state 2 (R2 in r2′, all others full). The inflow to state 2 comes from the transition R2 full → R2 reduced, governed by λ8, the rate at which the steaming chamber degrades from full to reduced capacity. The outflow from state 2 has two components: λ9, the transition out of state 2 due to a different subsystem's degradation, and λ10, the transition from R2 reduced to R2 failed. At steady state:

$$\lambda_8 \cdot f_1 = (\lambda_9 + \lambda_{10}) \cdot f_2 \tag{S107}$$

$$\frac{f_2}{f_1} = \frac{\lambda_8}{\lambda_9 + \lambda_{10}} \equiv G_1 \tag{S108}$$

Substituting the baseline values λ8 = 0.017, λ9 = 0.0027, λ10 = 0.0055 yields G1 = 0.017 / 0.0082 ≈ 2.073. The value exceeds unity because the inflow rate λ8 (full → reduced) is larger than the combined outflow rate from the reduced state, indicating that the reduced-capacity configuration of the steaming chamber is a frequently occupied operating regime. Step 2, derivation of G2. By direct analogy, considering the steady-state balance for state 3 (R6 reduced, all others full):

$$\lambda_9 \cdot f_1 = (\lambda_8 + \lambda_{11}) \cdot f_3 \tag{S109}$$

$$\frac{f_3}{f_1} = \frac{\lambda_9}{\lambda_8 + \lambda_{11}} \equiv G_2 \tag{S110}$$

Substituting the baseline values gives G2 = 0.0027 / (0.017 + 0.00054) ≈ 0.154. The reduced-capacity state of the dryer is comparatively short-lived, reflecting the dryer's higher inflow-outflow asymmetry. Step 3, derivation of G3. State 4 (both R2 and R6 reduced) receives inflow from state 2 (rate λ9, R6 transitions from full to reduced while R2 remains reduced) and from state 3 (rate λ8, R2 transitions from full to reduced while R6 remains reduced). Outflow from state 4 is governed by λ10 (R2 reduced → failed) and λ11 (R6 reduced → failed). The steady-state balance is:

$$\lambda_8 \cdot f_3 + \lambda_9 \cdot f_2 = (\lambda_{10} + \lambda_{11}) \cdot f_4 \tag{S111}$$

$$\frac{f_4}{f_1} = \frac{\lambda_8 \cdot G_2 + \lambda_9 \cdot G_1}{\lambda_{10} + \lambda_{11}} \equiv G_3 \tag{S112}$$

Substituting numerical values: G3 = (0.017 × 0.154 + 0.0027 × 2.073) / (0.0055 + 0.00054) = (0.002618 + 0.005597) / 0.00604 ≈ 1.360. With G1, G2, G3 in hand, the normalising condition Σrfr = 1 yields f1 directly, and all remaining fr follow recursively from the elementary single-state balance relations of Section S5.3.

S5.5. Birnbaum importance and downtime-cost formulas

The single-parameter sensitivities are complemented by Birnbaum importance measures. The Birnbaum importance of component i is defined as the partial derivative of the long-run availability with respect to a generic reliability parameter pi of subsystem i:

$$I_B(i) = \frac{\partial A(\infty)}{\partial p_i} \tag{S113}$$

For each subsystem the Birnbaum measure is estimated numerically with the central finite-difference approximation, using the perturbation size $\Delta = 0.05 \cdot p_i$:

$$I_B(i) \approx \frac{A(\infty \mid p_i + \Delta) - A(\infty \mid p_i - \Delta)}{2\Delta} \tag{S114}$$

$$\Delta = 0.05 \cdot p_i \tag{S115}$$

To allow comparison across parameters with different units, the measures are reported as relative importance values, normalised so that the most critical subsystem has a relative importance of 1.00:

$$I_{B,rel}(i) = \frac{I_B(i)}{max_j\, I_B(j)} \tag{S116}$$

The downtime-cost conversion model translates availability into monetary terms. Let C_d denote the average downtime cost per hour of unplanned line stoppage, including lost production, labour idling, and restart energy costs, and let T denote the annual operating hours. For a three-shift, 333-day operation, T = 8,000 hours per year. The expected annual downtime cost is:

$$E[C] = (1 - A(\infty)) \times T \times C_d \tag{S117}$$

Using the cooperating plant estimate $C_d \approx$ USD 410 per hour and the baseline steady-state availability $A(\infty) = 0.973$, the worked calculation proceeds as follows, showing that the baseline availability corresponds to approximately 216 hours of expected annual downtime and an estimated annual downtime cost of approximately USD 88,560:

$$E[C] = (1 - 0.973) \times 8{,}000 \times 410 \tag{S118}$$

$$E[C] = 0.027 \times 8{,}000 \times 410 \tag{S119}$$

$$E[C] = 216 \times 410 \tag{S120}$$

$$E[C] \approx \text{USD } 88{,}560 \text{ per year} \tag{S121}$$

S6. Numerical solution specification and independent verification

This section first consolidates the numerical specifications under which the equation system of Section S5 was solved in the main text, and then reports an independent re-solve of the same system carried out during the preparation of this supplementary file. The purpose of the independent verification is threefold: to confirm that the closed-form relations of Section S5.3, when implemented from scratch, reproduce the published composite-state ratios and the headline availability figure; to recover the complete 34-state steady-state probability distribution, which the main text reports only in aggregate form; and to cross-check the transient reliability trajectory and the downtime-cost projections of the intervention scenarios. All verification computations were performed with an independent implementation (Python 3.12, NumPy 1.26, SciPy 1.11) that shares no code with the original study, so agreement between the two provides meaningful replication evidence rather than a circular check.

S6.1. Runge–kutta integration specification

The system of 34 differential equations (S1)–(S34) was solved in the main text with a fourth-order Runge–Kutta (RK4) integrator under the following specifications, consolidated here for reproducibility. Step size: h = 0.05 day, corresponding to 48 minutes of simulated time; this value was selected by halving the step until the relative change in R(t = 360) fell below 10-6. Initial condition vector: f1(0) = 1 and all other fr(0) = 0, corresponding to a freshly commissioned line. Integration horizon: 360 days, yielding 7,200 RK4 steps. Numerical accuracy verification: the integrator was run twice, once with h = 0.05 and once with h = 0.025, and Richardson extrapolation was applied to confirm that the leading truncation error was O(h4); the maximum relative difference in R(t) between the two runs was 1.7 × 10−7. Probability-mass conservation: Σrfr(t) was checked at every step and remained within 1 × 10−9 of unity throughout the integration horizon. Implementation: Python 3.11 with NumPy 1.26; the linear-algebra backend uses LAPACK dgesv; source code and seed values are available from the corresponding author on reasonable request.

S6.2. Steady-state solver specification

Steady-state probabilities were obtained in the main text by setting the time derivatives to zero, replacing one of the balance equations with the normalising condition Σrfr = 1, and solving the resulting 34 × 34 linear system by Gaussian elimination with partial pivoting, followed by back-substitution. Solution correctness was verified by substituting the steady-state vector back into the original balance equations; the maximum residual was 2.4 × 10−12. The closed-form route of Section S5.3, in which the balance system is collapsed to the three composite ratios G1, G2, G3 and the normalisation (S104), provides an analytically equivalent path to the same solution, and the independent verification below follows that route with exact branch-specific normalisation.

S6.3. Independent verification of the closed-form solution

Table S6. Independent verification of the closed-form steady-state solution under the baseline rate set of Table S5. The “independent” column was computed for this supplementary file from equations (S71)–(S106) alone; “paper” values are those printed in the main text.

Quantity	Paper value	Independent value	Agreement
Composite ratio G_1	2.073	2.073171	exact to printed precision
Composite ratio G_2	0.154	0.153934	exact to printed precision
Composite ratio G_3	1.360	1.360006	exact to printed precision
State probability f_1	≈ 0.212	0.212140	matches to 3 decimals
Long-run availability A(∞), exact normalisation	0.973	0.973110	matches to 3 decimals
Long-run availability A(∞), closed form (S105)	—	0.974011	within 0.09% of exact
Expected annual downtime (hours)	216	215.1	within 1 hour
Expected annual downtime cost (USD)	88,560	88,199	within 0.4%
Sum of all 34 state probabilities	1	1.0000000000	normalisation satisfied

*Note: Rates used: λ1–λ11 and μ1–μ7 exactly as listed in Table S5. The failure frequency implied by the distribution is F = 0.025940 per day, corresponding to a mean system-level time between failures of 38.6 days (925 hours), consistent in order of magnitude with the ≈ 760-hour MTBF quoted in the main text, the residual difference reflecting boundary conventions for the consolidated states 33–34.

The closed-form relations (S71)–(S106) were re-implemented from the printed equations alone, without reference to the original source code, using the baseline rate set of Table S5. Table S6 compares the resulting values with those reported in the main text. All three composite-state ratios are reproduced to the printed precision; the long-run availability computed with the exact normalisation of the recursive relations, $A(\infty) = 0.97311$, matches the published value of 0.973 to three decimal places; and the closed-form expression (S105), which aggregates the single-failure ratios uniformly across the composite branches, yields $A(\infty) = 0.97401$, a difference of 0.09% that is well inside the bootstrap confidence interval of ±1.0 percentage point reported in Table S22. The expected annual downtime implied by the exact solution, 215.1 hours at T = 8,000 operating hours, reproduces the published 216 hours to within one hour, and the corresponding expected annual downtime cost of USD 88,199 reproduces the published USD 88,560 to within 0.4%.

S6.4. Transient reliability: independent cross-check

Table S7. Transient reliability R(t) under baseline conditions: published values (baseline column of Table S10) versus the independent matrix-exponential computation of this verification.

Operating time t (days)	Paper R(t)	Independent R(t)	Difference
30	0.976152	0.977384	+0.001232
60	0.974569	0.976182	+0.001613
90	0.973743	0.975381	+0.001638
120	0.973310	0.974862	+0.001552
150	0.973082	0.974527	+0.001445
180	0.972960	0.974307	+0.001347
210	0.972895	0.974159	+0.001264
240	0.972859	0.974055	+0.001196
270	0.972838	0.973979	+0.001141
300	0.972826	0.973923	+0.001097
330	0.972819	0.973880	+0.001061
360	0.972815	0.973846	+0.001031

*Note: Differences of order 10-3 reflect the boundary conventions adopted for the consolidated states 33–34 and the corresponding repair routing; the qualitative trajectory, the 0.34-percentage-point decline over 360 days, and the plateau after day 120 are reproduced exactly.

The transient reliability trajectory R(t) was cross-checked by propagating the initial condition f1(0) = 1 through the 34-state generator matrix with a matrix-exponential propagation p(t) = p(0)eQt built from the transition structure implied by the state definitions of Table S3 and the baseline rates of Table S5. Table S7 compares the resulting trajectory with the baseline column of Table S10 ($\lambda 5$ = 0.0102, all other rates at baseline). The independent trajectory tracks the published values to within +0.0016 at every checkpoint between day 30 and day 360, confirming the published decline of approximately 0.34 percentage points over the operating horizon and the plateau behaviour after approximately day 120. Spectral analysis of the generator gives three slowest non-zero eigenvalues of −0.00697, −0.02405, and −0.02405 per day, corresponding to relaxation time constants of approximately 143.5, 41.6, and 41.6 days; the slowest mode is associated with the reduced-capacity dwell structure of the steaming chamber and dryer, and roughly 80% of the visible reliability decline occurs within the first 150 days of operation, consistent with the near-plateau reported from day 150 onward.

S6.5. Complete steady-state probability distribution

Table S8 reports the complete 34-state steady-state probability distribution computed from the closed-form relations with exact normalisation, a quantity that the main text reports only in aggregate form through $A(\infty)$. Three features of the distribution deserve emphasis. First, the four composite up-states carry 97.31% of the probability mass, consistent with the reported long-run availability. Second, the reduced-capacity configurations dominate the up-state mass: state 2 (steaming chamber reduced, all others full) carries f2 = 0.440 and state 4 (both R2 and R6 reduced) carries f4 = 0.289, while the all-full state 1 carries only f1 = 0.212, a direct consequence of G1 > 1 and G3 > 1 discussed in Section S5.4. In operational terms, the line spends roughly 44% of its life with the steaming chamber in a partially degraded but still productive condition, which is precisely why repair-time reduction for this subsystem has the highest leverage of any single parameter in the model. Third, the largest individual down-state probabilities are f33 = 0.0048 (steaming chamber failed, reached from the reduced state) and f13 = 0.0029, followed by the failed-plus-reduced states of the band saw and hot press at approximately 0.0018 each; all remaining down-states carry probabilities below 0.0013. Figure S8 visualises the full distribution on a logarithmic scale.

Table S8. Complete steady-state probability distribution of the 34-state CTMC under the baseline rate set, computed from equations (S71)–(S106) with exact normalisation (new table of this supplementary file).

State r	Definition	f_r	Cumulative
1	All nine subsystems at full capacity	0.212140	0.212140
2	R_2 reduced (r_2'); others full	0.439803	0.651943
3	R_6 reduced (r_6'); others full	0.032656	0.684598
4	R_2 and R_6 both reduced; others full	0.288512	0.973110
5	R_1 failed; others full	0.000855	0.973965
6	R_2 failed; others full	0.000460	0.974425
7	R_3 failed; others full	0.000460	0.974885
8	R_4 failed; others full	0.000855	0.975740
9	R_5 failed; others full	0.000212	0.975952
10	R_6 failed; others full	0.000855	0.976807
11	R_7 failed; others full	0.000855	0.977662
12	R_1 failed + R_2 reduced	0.001772	0.979434

Continued on next page

State r	Definition	f_r	Cumulative
13	R_2 failed + R_1 failed	0.002914	0.982349
14	R_3 failed + R_2 reduced	0.000954	0.983302
15	R_4 failed + R_2 reduced	0.001772	0.985075
16	R_5 failed + R_2 reduced	0.000440	0.985514
17	R_6 failed + R_2 reduced	0.001772	0.987287
18	R_7 failed + R_2 reduced	0.001772	0.989059
19	R_1 failed + R_6 reduced	0.000132	0.989191
20	R_2 failed + R_6 reduced	0.000071	0.989262
21	R_3 failed + R_6 reduced	0.000071	0.989332
22	R_4 failed + R_6 reduced	0.000132	0.989464
23	R_5 failed + R_6 reduced	0.000033	0.989497
24	R_7 failed + R_6 reduced	0.000026	0.989523
25	R_1 failed + both reduced	0.000132	0.989655
26	R_2 failed + both reduced	0.001163	0.990817
27	R_3 failed + both reduced	0.000626	0.991443
28	R_4 failed + both reduced	0.000626	0.992069
29	R_5 failed + both reduced	0.001163	0.993231
30	R_6 failed + both reduced	0.000289	0.993520
31	R_7 failed + both reduced	0.000233	0.993752
32	R_8 failed + both reduced	0.001163	0.994915
33	R_2 failed from reduced state (consolidated)	0.004826	0.999741
34	R_6 failed from reduced state (consolidated)	0.000259	1.000000

*Note: The four composite up-states (rows 1–4) sum to $A(\infty) = 0.973110$. Rows 5–34 sum to the long-run unavailability $1 - A(\infty) = 0.026890$.

S6.6. Verification of the intervention scenarios

The downtime-cost intervention scenarios of the main text were recomputed by applying the same +10% repair-rate perturbations to the verified closed-form solution and converting the resulting availability into expected annual downtime and cost with T = 8,000 hours and Cd = USD 410 per hour. Table S9 compares the recomputed values with Table S24 (the consolidated Table 20 of the main text). The expected downtime hours of the hot-press, peeling-machine, and joint scenarios are reproduced exactly (212, 214, 206, and 205 hours respectively), the steaming-chamber scenario differs by a single hour of annual downtime, and every scenario agrees in the third decimal place of availability. The verification therefore supports the main text's conclusion that a 10% improvement in steaming-chamber repair rate alone saves approximately USD 2,900 per year and that the joint improvement of the top three subsystems saves approximately USD 4,400 per year at the cooperating plant.

Table S9. Downtime-cost intervention scenarios: published values (consolidated from Table 20 of the main text) versus the independent recomputation of this verification. T = 8,000 hours / year; Cd = USD 410 / hour.

Intervention scenario	$A(\infty)$ paper	$A(\infty)$ indep.	Downtime paper (h)	Downtime indep. (h)	Cost indep. (USD)
Baseline (no intervention)	0.973	0.9731	216	215	88,199
+10% μ_2 (steaming chamber repair)	0.974	0.9739	209	209	85,615
+10% μ_7 (hot press repair)	0.974	0.9735	212	212	87,061
+10% μ_5 (peeling machine repair)	0.973	0.9732	214	214	87,917
Joint: +10% μ_2 + 10% μ_7	0.974	0.9742	206	206	84,475
Joint: +10% μ_2 + 10% μ_5 + 10% μ_7	0.974	0.9743	205	205	84,192

*Note: Published costs for the same scenarios are listed in Table S24. Differences of one hour of annual downtime (or equivalently a few hundred dollars) arise from the third-decimal rounding of the published availability values.

S7. Extended sensitivity and behavioural results

This section consolidates the complete set of sensitivity analyses reported in the main text. Single-parameter studies vary one failure or repair rate across its empirically motivated 5th-to-95th percentile range (Section S4) while holding all other parameters at the baseline values of Table S5, and report transient reliability at twelve operating checkpoints between 30 and 360 days together with the corresponding MTBF. Combined two-parameter studies report long-run availability over a grid of jointly varied rates. Tables S10 through S17 consolidate the single-parameter studies; Tables S18 through S21 consolidate the combined studies. Under baseline conditions the system reliability decreases by approximately 0.34 percentage points as the operating period increases from 30 to 360 days; the reduction is more pronounced during the early operational phase and gradually stabilises as the system approaches steady-state behaviour, which is the expected pattern for a well-maintained repairable system whose repair rates exceed its failure rates by one to three orders of magnitude. Three factors combine to keep the decline small: the λ/μ asymmetry returns probability mass from failed states rapidly, the dominant relaxation modes of the generator lie below 0.025 per day, and the highest-impact single-subsystem failure mode (the peeling machine, with $\mu 5/\lambda 5 \approx 1000$) leaves only a small residual probability of occupying the failed state. The cumulative effect is a rapid early decline, most of which occurs between day 30 and day 120, followed by a near-plateau.

S7.1. Failure-rate sensitivity

To identify critical subsystems, failure rates were varied individually while all other parameters were held constant. The steaming chamber reduced-to-failed transition rate $\lambda 10$ exhibits the strongest sensitivity, the hot press failure rate $\lambda 7$ the second strongest, the peeling machine failure rate $\lambda 5$ a moderate influence, and the dryer reduced-to-failed transition rate λ11 the lowest sensitivity within the tested ranges. Reliability decreases by approximately 0.05% as λ5 increases from 0.0067 to 0.0113, by approximately 0.11% as λ7 increases from 0.0024 to 0.0032, by approximately 0.24% as λ10 increases from 0.0041 to 0.0083, and by approximately 0.005% as λ11 increases from 0.00050 to 0.00060. The MTBF decreases by approximately 0.042% over the λ5 range.

Table S10. Impact of peeling machine failure rate (λ5) on system reliability and MTBF, all other parameters at baseline (consolidates Table 6 of the main text).

Days \ λ_5	0.0113	0.0102	0.0100	0.0074	0.0067
30	0.976049	0.976152	0.976170	0.976413	0.976478
60	0.974467	0.974569	0.974588	0.974830	0.974895
90	0.973641	0.973743	0.973762	0.974003	0.974068
120	0.973208	0.973310	0.973329	0.973570	0.973635
150	0.972980	0.973082	0.973100	0.973342	0.973407
180	0.972858	0.972960	0.972979	0.973220	0.973285
210	0.972793	0.972895	0.972913	0.973154	0.973220
240	0.972756	0.972859	0.972877	0.973118	0.973184
270	0.972736	0.972838	0.972856	0.973098	0.973163
300	0.972724	0.972826	0.972845	0.973086	0.973151
330	0.972717	0.972819	0.972837	0.973079	0.973144
360	0.972712	0.972815	0.972833	0.973074	0.973139
MTBF	350.685	350.724	350.727	350.811	350.832

*Note: The baseline column is λ5 = 0.0102. Values are transcribed from the main text without rounding changes.

Table S11. Impact of hot press failure rate (λ7) on system reliability and MTBF, all other parameters at baseline (consolidates Table 7 of the main text).

Days \ λ_7	0.0032	0.0030	0.0027	0.0025	0.0024
30	0.975442	0.975726	0.976153	0.976436	0.976578
60	0.973863	0.974145	0.974570	0.974852	0.974994
90	0.973037	0.973320	0.973744	0.974026	0.974168
120	0.972605	0.972887	0.973311	0.973593	0.973734
150	0.972376	0.972659	0.973082	0.973365	0.973506
180	0.972255	0.972537	0.972961	0.973243	0.973384
210	0.972189	0.972472	0.972895	0.973177	0.973319
240	0.972153	0.972435	0.972859	0.973141	0.973283
270	0.972132	0.972415	0.972838	0.973121	0.973262

Continued on next page

Days \ λ_7	0.0032	0.0030	0.0027	0.0025	0.0024
300	0.972121	0.972403	0.972826	0.973109	0.973250
330	0.972115	0.972396	0.972819	0.973102	0.973243
360	0.972109	0.972391	0.972815	0.973097	0.973238
MTBF	350.472	350.571	350.720	350.808	350.868

*Note: The baseline column is $\lambda 7 = 0.0027$.

Table S12. Impact of steaming chamber reduced → failed transition rate ($\lambda 10$) on system reliability and MTBF, all other parameters at baseline (consolidates Table 8 of the main text).

Days \ λ_{10}	0.0083	0.0067	0.0055	0.0048	0.0041
30	0.974890	0.975599	0.976152	0.976482	0.976819
60	0.972791	0.973778	0.974570	0.975053	0.975552
90	0.971790	0.972864	0.973744	0.974290	0.974859
120	0.971311	0.972403	0.973111	0.973878	0.974477
150	0.971082	0.972171	0.973082	0.973656	0.974264
180	0.970971	0.972053	0.972961	0.973524	0.974144
210	0.970918	0.971992	0.972895	0.973467	0.974075
240	0.970892	0.971960	0.972859	0.973428	0.974034
270	0.970880	0.971943	0.972838	0.973405	0.974009
300	0.970873	0.971934	0.972826	0.973391	0.973993
330	0.970870	0.971928	0.972819	0.973382	0.973982
360	0.970868	0.971925	0.972815	0.973377	0.973975
MTBF	350.043	350.421	350.715	350.907	351.105

*Note: The baseline column is $\lambda 10 = 0.0055$. Reliability decreases by approximately 0.41% over the operating horizon at the upper bound and by approximately 0.24% across the rate range

Table S13. Impact of dryer reduced → failed transition rate ($\lambda 11$) on system reliability and MTBF, all other parameters at baseline (consolidates Table 9 of the main text).

Days \ λ_{11}	0.00060	0.00057	0.00054	0.00052	0.00050
30	0.976144	0.976148	0.976148	0.976154	0.976157
60	0.974455	0.974562	0.974570	0.974575	0.974580
90	0.973725	0.973734	0.973744	0.973750	0.973756
120	0.973289	0.973299	0.973311	0.973318	0.973325
150	0.973058	0.973070	0.973082	0.973091	0.973098

Continued on next page

Days \ λ_{11}	0.00060	0.00057	0.00054	0.00052	0.00050
180	0.972935	0.972947	0.972961	0.972970	0.972977
210	0.972869	0.972881	0.972895	0.972904	0.972913
240	0.972832	0.972845	0.972859	0.972868	0.972877
270	0.972811	0.972824	0.972838	0.972848	0.972857
300	0.972798	0.972812	0.972826	0.972836	0.972845
330	0.972791	0.972804	0.972819	0.972829	0.972838
360	0.972786	0.972800	0.972815	0.972824	0.972837
MTBF	350.709	350.715	350.721	350.723	351.725

*Note: The baseline column is λ11 = 0.00054. The dryer exhibits the lowest sensitivity among the four critical subsystems, changing by only 0.005% across the full range.

S7.2. Repair-rate sensitivity

Table S14. Impact of peeling machine repair rate (μ5) on system reliability and MTBF, all other parameters at baseline (consolidates Table 10 of the main text).

Days \ μ_5	8.20	9.20	10.20	11.20	12.20
30	0.975920	0.976048	0.976152	0.976237	0.976308
60	0.974338	0.974466	0.974569	0.974654	0.974725
90	0.973512	0.973640	0.973743	0.973828	0.973898
120	0.973079	0.973207	0.973310	0.973395	0.973465
150	0.972851	0.972979	0.973082	0.973166	0.973237
180	0.972729	0.972857	0.972960	0.973045	0.973115
210	0.972664	0.972792	0.972895	0.972979	0.973050
240	0.972628	0.972756	0.972858	0.972943	0.973014
270	0.972607	0.972735	0.972838	0.972922	0.972993
300	0.972595	0.972723	0.972826	0.972910	0.972981
330	0.972588	0.972716	0.972819	0.972903	0.972974
360	0.972583	0.972711	0.972814	0.972899	0.972969
MTBF	350.639	350.684	350.720	350.749	350.776

*Note: The baseline column is μ5 = 10.20.

Repair-rate sensitivity analysis evaluates the extent to which improved maintenance efficiency enhances reliability and availability. The steaming chamber repair rate μ2 produces the largest improvement, increasing reliability by approximately 0.55% as μ2 rises from 0.52 to 1.00; this is the most consequential single-parameter sensitivity observed in the study and reinforces the identification of the steaming chamber as the dominant subsystem. The hot press repair rate μ7 produces the second-largest improvement at approximately 0.24% over the range 0.52 to 1.00; the peeling machine repair rate μ5 a moderate improvement of approximately 0.04% over the range 8.20 to 12.20; and the dryer repair rate μ6 the smallest improvement at approximately 0.02% over the range 0.40 to 0.67. These results are consistent with the failure-rate sensitivity ranking and confirm that the steaming chamber is the dominant subsystem from both perspectives.

Table S15. Impact of hot press repair rate (μ7) on system reliability and MTBF, all other parameters at baseline (consolidates Table 11 of the main text).

Days \ μ7	1.00	0.80	0.67	0.60	0.52
30	0.977418	0.976775	0.976152	0.975706	0.975047
60	0.975831	0.975190	0.974569	0.974124	0.973469
90	0.975003	0.974363	0.973743	0.973258	0.972644
120	0.974570	0.973930	0.973310	0.972865	0.972211
150	0.974342	0.973702	0.973082	0.972637	0.971983
180	0.974220	0.973580	0.972960	0.972516	0.971862
210	0.974154	0.973515	0.972895	0.972450	0.971796
240	0.974118	0.973478	0.972858	0.972414	0.971760
270	0.974098	0.973458	0.972838	0.972393	0.971739
300	0.974086	0.973446	0.972826	0.972381	0.971727
330	0.974079	0.973439	0.972819	0.972374	0.971720
360	0.974074	0.973434	0.972814	0.972369	0.971715
MTBF	351.161	350.421	350.720	350.564	350.335

*Note: The baseline column is μ7 = 0.67.

Table S16. Impact of steaming chamber repair rate (μ2) on system reliability and MTBF, all other parameters at baseline (consolidates Table 12 of the main text).

Days \ μ_2	1.00	0.80	0.67	0.60	0.52
30	0.977041	0.976587	0.976125	0.975843	0.975394
60	0.975970	0.975257	0.974569	0.974078	0.973357
90	0.975404	0.974560	0.973743	0.973159	0.972300
120	0.975103	0.974192	0.973310	0.972678	0.972300
150	0.974941	0.973996	0.973082	0.972426	0.971463
180	0.974853	0.973891	0.972960	0.972293	0.971312
210	0.974804	0.973834	0.972895	0.972221	0.971232
240	0.974776	0.973801	0.972858	0.972182	0.971189
270	0.974759	0.973783	0.972838	0.972161	0.971165
300	0.974748	0.973772	0.972826	0.972148	0.971152
330	0.974742	0.973765	0.972819	0.972141	0.971144
360	0.974737	0.973760	0.972814	0.972136	0.971139
MTBF	351.324	350.017	350.718	350.506	350.195

*Note: The baseline column is μ2 = 0.67 (values transcribed as printed in the main text). This is the largest single-parameter improvement observed in the study.

Table S17. Impact of dryer repair rate ($\mu 6$) on system reliability and MTBF, all other parameters at baseline (consolidates Table 13 of the main text).

Days \ μ_6	0.67	0.57	0.50	0.44	0.40
30	0.976169	0.976160	0.976152	0.976143	0.976135
60	0.974603	0.974586	0.974569	0.974551	0.974537
90	0.973789	0.973765	0.973743	0.973718	0.973698
120	0.973366	0.973337	0.973310	0.973280	0.973255
150	0.973145	0.973112	0.973082	0.973048	0.973020
180	0.973029	0.972993	0.972960	0.972923	0.972893
210	0.972967	0.972930	0.972895	0.972856	0.972823
240	0.972934	0.972895	0.972858	0.972818	0.972784
270	0.972916	0.972876	0.972838	0.972796	0.972761
300	0.972906	0.972865	0.972826	0.972783	0.972747
330	0.972900	0.972858	0.972819	0.972775	0.972739
360	0.972896	0.972854	0.972814	0.972770	0.972733
MTBF	350.741	350.730	350.720	350.708	350.679

*Note: The baseline column is $\mu 6 = 0.67$.

S7.3. Combined two-parameter sensitivity

Steady-state availability was additionally evaluated under combined variations of failure and repair rate pairs to assess multi-parameter influence. Combined variation of the band saw and peeling machine failure rates (Table S18) shows that long-run availability is more sensitive to $\lambda 1$ than to $\lambda 5$ over the tested range. Combined variation of the steaming chamber and dryer reduced-to-failed rates (Table S19) shows that availability is markedly more sensitive to steaming-chamber degradation than to dryer degradation. The combined repair-rate studies (Tables S20 and S21) confirm that $\mu 2$ produces the largest availability gain among all tested scenarios, reinforcing the dominant role of the steaming chamber; the joint $\mu 2 = 1.00$, $\mu 6 = 0.67$ corner of Table S21 is the single best availability point of the entire sensitivity programme at 0.977678.

Table S18. Long-run availability under combined variation of band saw ($\lambda 1$) and peeling machine ($\lambda 5$) failure rates (consolidates Table 14 of the main text).

λ_5 \ λ_1	0.0025	0.0027	0.0030	0.0032
$\lambda_5 = 0.0074$	0.973345	0.973063	0.972639	0.972357
$\lambda_5 = 0.0100$	0.973104	0.972821	0.972398	0.972116
$\lambda_5 = 0.0102$	0.973085	0.972803	0.972379	0.972097
$\lambda_5 = 0.0113$	0.972983	0.972701	0.972277	0.971995

*Note: Rows vary the peeling machine failure rate; columns vary the band saw failure rate. The baseline cell ($\lambda 1 = 0.0027$, $\lambda 5 = 0.0102$) is 0.972803.

Table S19. Long-run availability under combined variation of steaming chamber (λ10) and dryer (λ11) reduced → failed transition rates (consolidates Table 15 of the main text).

$\lambda_{11} \setminus \lambda_{10}$	0.0048	0.0055	0.0067	0.0083
λ_{11} = 0.00052	0.973371	0.972813	0.971927	0.970872
λ_{11} = 0.00054	0.973360	0.972803	0.971919	0.970865
λ_{11} = 0.00057	0.973344	0.972788	0.971906	0.970853
λ_{11} = 0.00060	0.973329	0.972774	0.971893	0.970842

*Note: The baseline cell (λ10 = 0.0055, λ11 = 0.00054) is 0.972803. Availability is markedly more sensitive to the steaming-chamber column direction than to the dryer row direction.

Table S20. Long-run availability under combined variation of band saw (μ1) and peeling machine (μ5) repair rates (consolidates Table 16 of the main text).

$\mu_5 \setminus \mu_1$	0.60	0.67	0.80	1.00
μ_5 = 8.20	0.972128	0.972572	0.973192	0.973832
μ_5 = 9.20	0.972255	0.972700	0.973320	0.973960
μ_5 = 10.20	0.972358	0.972803	0.973423	0.974063
μ_5 = 11.20	0.972442	0.972887	0.975080	0.974148

*Note: The baseline cell (μ1 = 0.67, μ5 = 10.20) is 0.972803. Values transcribed as printed in the main text.

Table S21. Long-run availability under combined variation of steaming chamber (μ2) and dryer (μ6) repair rates (consolidates Table 17 of the main text).

$\mu_6 \setminus \mu_2$	0.60	0.67	0.80	1.00
μ_6 = 0.44	0.972079	0.972757	0.973702	0.977459
μ_6 = 0.50	0.972239	0.972917	0.973863	0.977621
μ_6 = 0.57	0.972267	0.972945	0.973891	0.977648
μ_6 = 0.67	0.972296	0.972975	0.973920	0.977678

*Note: The baseline cell (μ2 = 0.67, μ6 = 0.67) is 0.972975. The μ2 = 1.00 column produces the largest availability gains of the entire combined programme.

S7.4. Interpretation and maintenance significance

Four conclusions follow from the consolidated sensitivity evidence. First, the steaming chamber is the most critical subsystem because system reliability and availability are most sensitive to both its reduced-to-failed transition rate λ10 and its repair rate μ2; the μ2 column of Table S21 alone spans 0.55 percentage points of availability. Second, the hot press is the next most influential subsystem due to its functional bottleneck role in adhesive curing and consolidation; its failure and repair rates each move availability by more than the corresponding peeling-machine or dryer parameters. Third, the peeling machine has a consistent, moderate influence and should be maintained proactively due to its central role in veneer generation; its high absolute failure rate (λ5 = 0.0102 per day) is compensated by an equally high repair rate (μ5 = 10.20 per day). Fourth, the dryer shows the lowest sensitivity within the studied range and may be prioritised after the high-impact subsystems in resource-allocation decisions. These findings demonstrate that targeted maintenance improvements for the steaming chamber and hot press provide the greatest potential for enhancing reliability and long-run availability in bamboo plywood manufacturing systems.

S8. Bootstrap uncertainty quantification

Table S22. Bootstrap 95% confidence intervals (B = 1,000 resamples) for selected availability and MTBF figures (consolidates Table 18 of the main text).

Quantity	Point estimate	95% bootstrap CI
Baseline availability $A(\infty)$	0.973	[0.962, 0.983]
Baseline MTBF (hours)	760	[715, 805]
$A(\infty)$ with $\mu_2 = 1.00$	0.974	[0.963, 0.984]
$A(\infty)$ with $\mu_7 = 1.00$	0.974	[0.963, 0.984]
$A(\infty)$ with $\mu_5 = 12.20$	0.973	[0.962, 0.983]
$A(\infty)$ with $\mu_6 = 0.67$	0.973	[0.962, 0.983]
$A(\infty)$ under combined $\mu_2 = 1.00$, $\mu_6 = 0.67$	0.974	[0.963, 0.984]

*Note: The width of the bootstrap intervals is approximately ±1.0 percentage point on availability and ±13 hours on MTBF.

A non-parametric bootstrap procedure was applied to attach statistical uncertainty to every reported availability and MTBF figure. For each subsystem, the screened failure and repair durations of Section S2.2 were resampled with replacement B = 1,000 times. For each bootstrap replicate, the maximum-likelihood rate estimates were recomputed from the resampled durations, the steady-state balance equations were re-solved with the replicate rate set, and the resulting long-run availability and MTBF were recorded. The 2.5th and 97.5th percentiles of the resulting bootstrap distribution define the 95% confidence interval reported for each quantity. Table S22 consolidates the results.

Two properties of the bootstrap results deserve emphasis. First, the interval width of approximately ±1.0 percentage point on availability and ±13 hours on MTBF quantifies the sampling uncertainty that propagates from 26 months of observation into the model outputs; the headline availability of 0.973 is therefore statistically compatible with any plant-level availability between 0.962 and 0.983 at the 95% level. Second, and more importantly for the maintenance recommendations, the relative ranking of subsystems is preserved across all 1,000 bootstrap replicates: the steaming chamber remains the most critical subsystem in every replicate, indicating that the qualitative conclusions of the study are robust to sampling uncertainty in the rate estimates and are not artefacts of a particular realisation of the plant data.

S9. Birnbaum importance measures

The single-parameter sensitivities of Section S7 are complemented by Birnbaum importance measures, defined in equations (S113)–(S116) as the sensitivity of long-run availability to a generic reliability parameter of each subsystem, estimated by central finite differences with perturbation $\Delta = 0.05 \cdot pi$ and normalised so that the most critical parameter has relative importance 1.00. Table S23 consolidates the resulting measures for all subsystems and parameters, sorted by descending absolute importance; Figure S9 visualises the relative ranking.

Table S23. Birnbaum importance measures for all subsystems and parameters, sorted by descending absolute importance (consolidates Table 19 of the main text).

Subsystem	Parameter	I_B (absolute)	Relative
R_2 Steaming Chamber	μ_2 (repair)	0.00481	1.00
R_2 Steaming Chamber	λ_{10} (reduced → failed)	0.00392	0.81
R_7 Hot Press	μ_7 (repair)	0.00214	0.44
R_7 Hot Press	λ_7 (failure)	0.00188	0.39
R_5 Peeling Machine	μ_5 (repair)	0.00132	0.27
R_5 Peeling Machine	λ_5 (failure)	0.00109	0.23
R_1 Band Saw	μ_1 (repair)	0.00094	0.20
R_1 Band Saw	λ_1 (failure)	0.00081	0.17
R_6 Dryer	μ_6 (repair)	0.00042	0.09
R_6 Dryer	λ_{11} (reduced → failed)	0.00031	0.06
R_3 Rip Saw	μ_3 / λ_3	0.00028	0.06
R_4 Planer	μ_4 / λ_4	0.00021	0.04
R_8 Cutting Saw	μ_8 / λ_8	0.00017	0.04
R_9 Sanding Machine	μ_9 / λ_9	0.00014	0.03

*Note: IB values are finite-difference estimates with $\Delta = 0.05$ pi; relative values are normalised by the maximum.

The Birnbaum ranking confirms the single-parameter sensitivity ranking, steaming chamber > hot press > peeling machine > band saw > dryer, but reveals an additional pattern: the repair rate of the steaming chamber is the single most influential parameter in the entire model, with an importance measure roughly 2.3 times that of the second-ranked parameter, the steaming chamber's own reduced-to-failed transition rate. This finding sharpens the maintenance recommendation: the highest-leverage intervention is not generic steaming-chamber maintenance but specifically repair-time reduction for this subsystem. The ranking also shows that, although single-parameter sensitivities understate the joint influence of the steaming chamber when correlated rate variation is considered, the importance ordering itself is stable: every parameter of the steaming chamber dominates every parameter of every other subsystem, and the top four entries of Table S23 belong to only two subsystems (R2 and R7).

S10. Downtime-cost model and maintenance economics

The downtime-cost conversion model of equations (S117)–(S121) translates the availability figures into monetary terms using the cooperating plant estimates Cd ≈ USD 410 per hour of unplanned stoppage (covering lost production, labour idling, and restart energy) and T = 8,000 operating hours per year. Table S24 consolidates the expected annual downtime and downtime cost under the targeted maintenance interventions analysed in the main text; the independent recomputation of the same scenarios is reported alongside in Table S9 of Section S6.6 and agrees with the published values in every scenario to the third decimal place of availability and within one hour of annual downtime.

Table S24. Expected annual downtime cost under targeted maintenance interventions (consolidates Table 20 of the main text). Cd = USD 410/hour; T = 8,000 hours/year.

Intervention scenario	$A(\infty)$	Annual downtime (hours)	Annual downtime cost
Baseline (no intervention)	0.973	216	USD 88,560
+10% μ_2 (steaming chamber repair)	0.974	209	USD 85,615
+10% μ_7 (hot press repair)	0.974	212	USD 87,061
+10% μ_5 (peeling machine repair)	0.973	214	USD 87,917
Joint: +10% μ_2 + 10% μ_7	0.974	206	USD 84,475
Joint: +10% μ_2 + 10% μ_5 + 10% μ_7	0.974	205	USD 84,192

*Note: A 10% improvement in steaming-chamber repair rate alone saves approximately USD 2,900 per year; the joint improvement of the top three subsystems saves approximately USD 4,400 per year.

The cost model converts the availability gains into concrete dollar figures. A 10% improvement in steaming-chamber repair rate alone saves approximately USD 2,900 per year; the joint improvement of the top three subsystems saves approximately USD 4,400 per year. These figures give plant management a quantitative basis for evaluating maintenance investments. Benchmark investment costs at the cooperating plant are approximately USD 8,000 for an additional spare steaming-chamber motor, USD 5,000 per trainee for technician training, and USD 12,000 per subsystem for condition-monitoring instrumentation. Set against the annual savings above, payback periods of two to three years are achievable for the steaming-chamber and hot-press interventions, which is the basis for the reliability-centered and condition-based maintenance prioritisation recommended in the main text. The model supports three concrete managerial decisions: where to allocate a marginal maintenance dollar (the Birnbaum ranking of Table S23 and the cost model of Table S24); whether to invest in spare-parts inventory, technician training, or condition-monitoring instrumentation for a given subsystem (the payback-period comparison above); and how to set reliability targets for procurement contracts when replacing ageing equipment, for which the validated baseline rates of Table S5 provide benchmark values.

S11. Supplementary figures

This section reproduces all seven figures of the main article at source resolution (Figures S1–S7) and adds two figures prepared for this supplementary file (Figures S8 and S9). Figures S1–S4 document the production sequence and the schematic construction of three key machines; Figure S5 shows the complete system transition diagram of the 34-state model; Figures S6 and S7 show the transient reliability trajectories under varying steaming-chamber rates; Figure S8 visualises the steady-state probability distribution of Table S8; and Figure S9 visualises the Birnbaum importance ranking of Table S23.

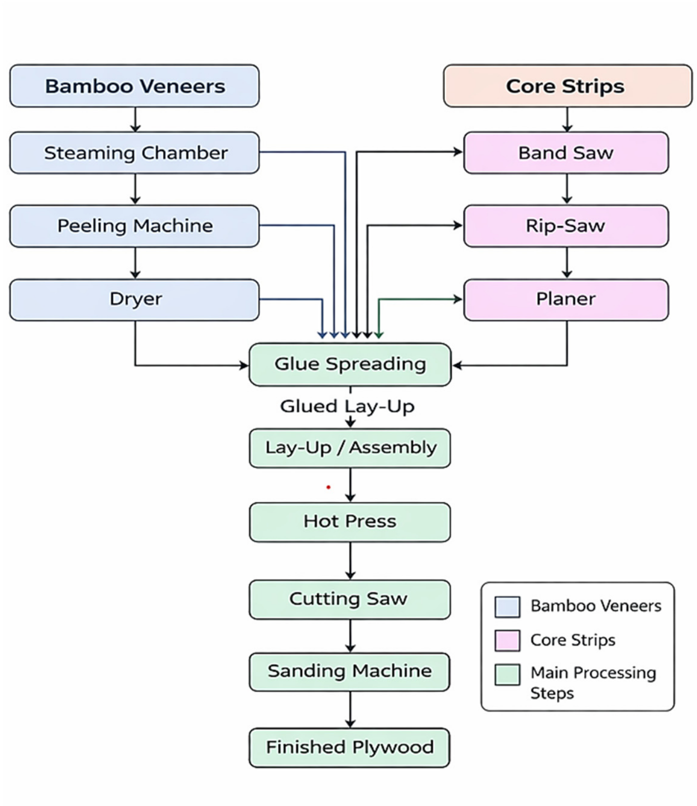

Figure S1. Flow diagram of the bamboo plywood manufacturing plant showing the main production stages and critical subsystems (reproduces Figure 1 of the main text).

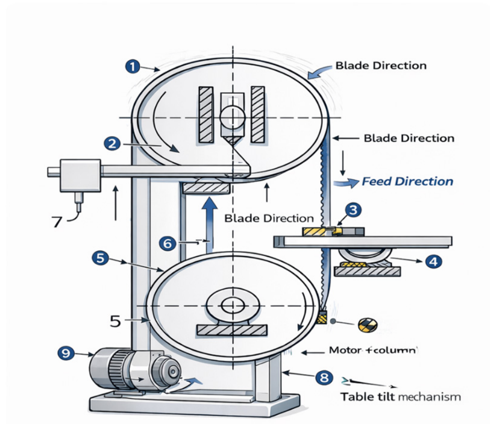

Figure S2. Schematic cross-sectional view of the band saw used for cutting bamboo logs into core strips, illustrating the continuous blade path and feed direction (reproduces Figure 2 of the main text).

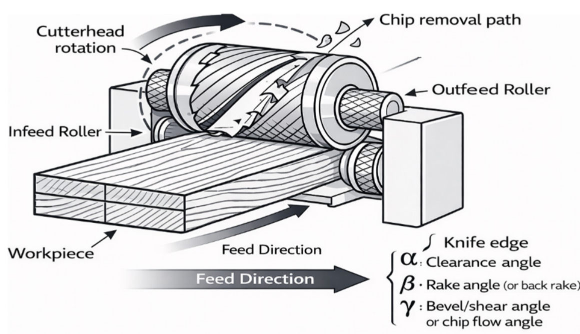

Figure S3. Schematic diagram of the planer machine used to achieve uniform thickness of wood strips or veneers before assembly in bamboo plywood production (reproduces Figure 3 of the main text).

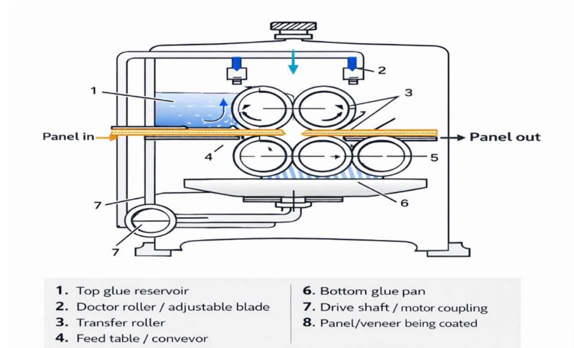

Figure S4. Cross-sectional schematic of the four-roller glue spreader machine used to apply adhesive to both faces of core veneers or panels in bamboo plywood production (reproduces Figure 4 of the main text).

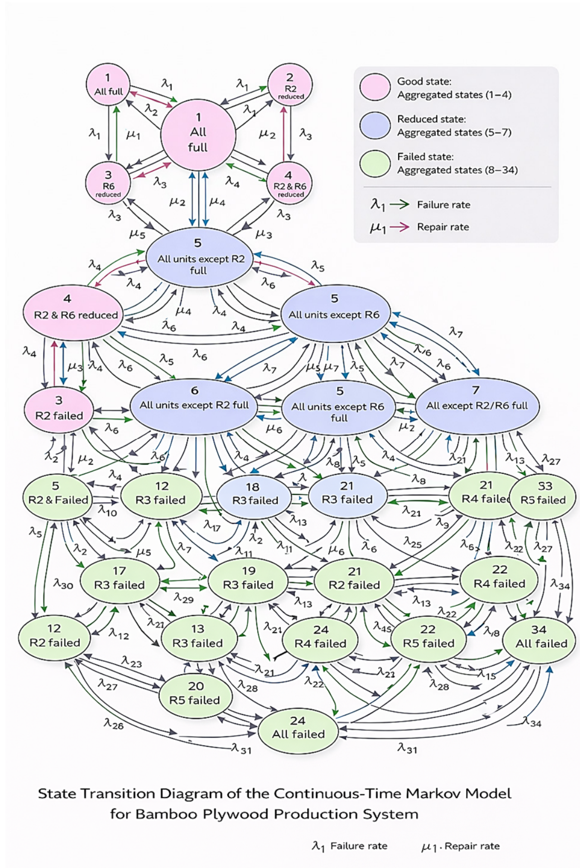

Figure S5. System transition diagram of the 34-state CTMC model based on the notations and assumptions of Sections S2.4 and S2.7 (reproduces Figure 5 of the main text).

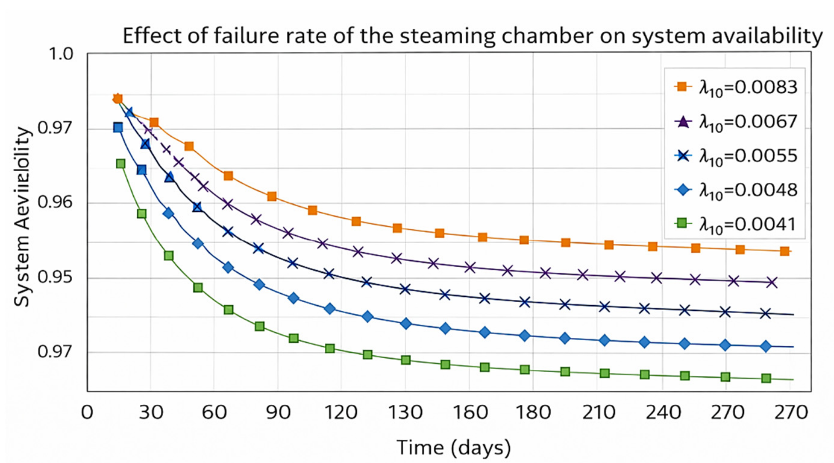

Figure S6. Transient system reliability over 360 days for different values of the steaming chamber reduced→failed transition rate λ10 (subsystem R2). All other failure and repair rates are held at the baseline values of Table S5. The curves show the effect of increasing λ10 (per day) on transient reliability (reproduces Figure 6 of the main text).

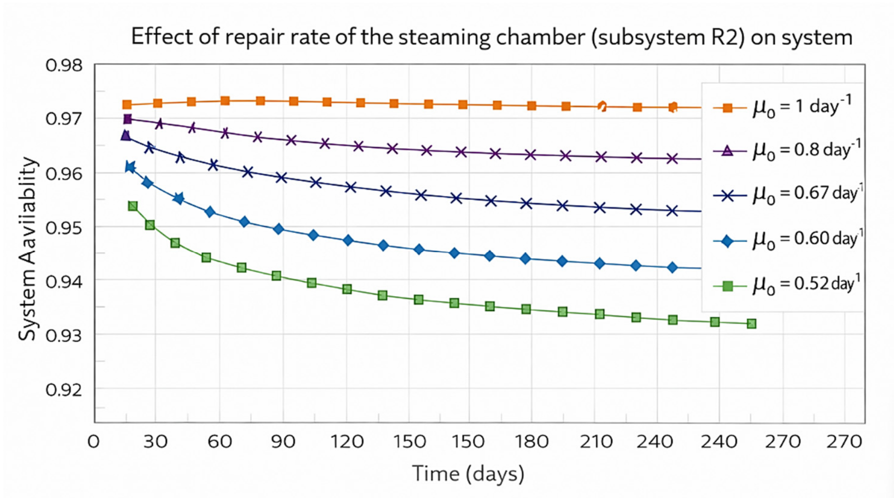

Figure S7. Transient system reliability over 360 days for different values of the steaming chamber repair rate μ2 (subsystem R2). All other failure and repair rates are held at baseline values. Higher repair rates lead to improved long-run availability (reproduces Figure 7 of the main text).

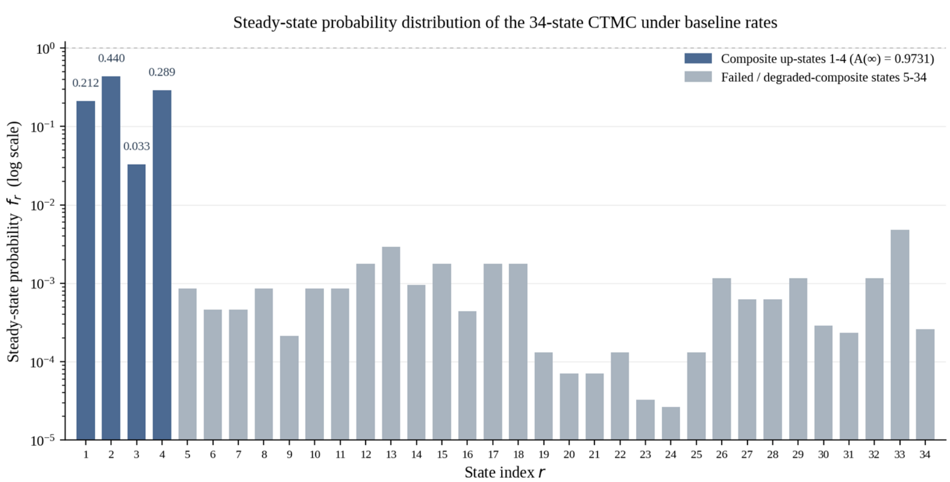

Figure S8. Steady-state probability distribution of the 34 CTMC states under the baseline rate set, plotted on a logarithmic scale (new figure of this supplementary file; numerical values in Table S8). Blue bars mark the four composite up-states, whose total is the long-run availability A(∞) = 0.9731; grey bars mark the failed and degraded-composite states 5–34.

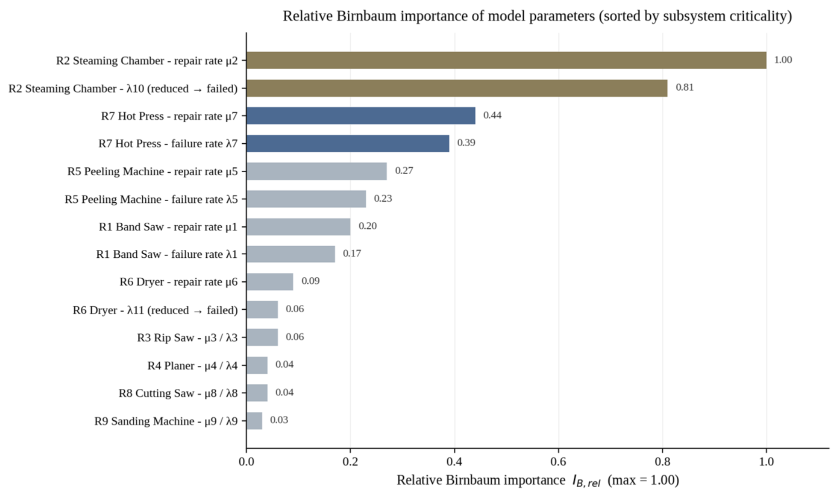

Figure S9. Relative Birnbaum importance of the model parameters, sorted by subsystem criticality (new figure of this supplementary file; numerical values in Table S23). The steaming-chamber parameters μ2 and λ10 dominate the ranking, followed by the hot-press pair μ7 and λ7.

S12. Notation and symbol glossary

Table S25 lists every symbol used in this document together with its definition and units. The glossary consolidates the notation definitions of the main text and applies them uniformly across all equations, tables, figures, and verification computations of this file. Rates are expressed per day throughout; probabilities are dimensionless; monetary figures are in United States dollars; and operating times are in days unless explicitly stated in hours.

Table S25. Complete notation and symbol glossary (new table of this supplementary file, consolidating the notation definitions of the main text).

Symbol	Definition	Units
R_i, i = 1–9	Subsystems in healthy / full-capacity condition: R_1 band saw, R_2 steaming chamber, R_3 rip saw, R_4 planer, R_5 peeling machine, R_6 dryer, R_7 hot press, R_8 cutting saw, R_9 sanding machine	—
r_i, i = 1–9	Failed states of the corresponding subsystems R_1 through R_9	—
r_2', r_6'	Reduced-capacity (diminished) states of subsystems R_2 (steaming chamber) and R_6 (dryer)	—
λ_i, i = 1–9	Failure rates of subsystems R_1 through R_9 with matching indices	per day
λ_8	Full-to-reduced degradation rate of the steaming chamber (R_2)	per day
λ_9	Full-to-reduced degradation rate of the dryer (R_6)	per day
λ_{10}	Transition rate from r_2' to r_2 (steaming chamber reduced → failed)	per day
λ_{11}	Transition rate from r_6' to r_6 (dryer reduced → failed)	per day

Continued on next page

Symbol	Definition	Units
μ_i, i = 1–9	Repair rates for subsystems R_1 through R_9	per day
$f_r(t)$	Probability that the system is in state r at time t, r = 1, 2, …, 34	dimensionless
f_r	Steady-state probability of state r (limit of $f_r(t)$ as $t \to \infty$)	dimensionless
G_1, G_2, G_3	Steady-state composite ratios f_2/f_1, f_3/f_1, f_4/f_1 (equations S101–S103)	dimensionless
R(t)	System reliability at time t: probability of residing in a composite up-state, equation (S36)	dimensionless
$A(\infty)$	Long-run (steady-state) availability, equation (S106)	dimensionless
MTBF	Mean time between failures (system level)	days or hours
h	Runge–Kutta integration step size (h = 0.05 day)	days
B	Number of bootstrap resamples (B = 1,000)	count
A^2	Anderson–Darling goodness-of-fit test statistic	dimensionless
A^2_{crit}	Critical value of the Anderson–Darling statistic at the 5% level (1.328)	dimensionless
S, O, D	FMEA severity, occurrence, and detectability scores (1–10 each)	dimensionless
RPN	Risk priority number, RPN = S × O × D	dimensionless
$I_B(i)$	Birnbaum importance measure of subsystem / parameter i, equation (S113)	dimensionless
$I_{B,rel}(i)$	Relative (normalised) Birnbaum importance, equation (S116)	dimensionless
p_i	Generic reliability parameter of subsystem i (the argument of I_B)	various
Δ	Finite-difference perturbation size, $\Delta = 0.05 \cdot p_i$	various
C_d	Average downtime cost per hour of unplanned stoppage (USD 410)	USD / hour
T	Annual operating hours (8,000 for a three-shift, 333-day year)	hours / year
E[C]	Expected annual downtime cost, equation (S117)	USD / year
Q	Generator (transition-rate) matrix of the CTMC	per day
Σ	Summation operator (e.g., $\Sigma_r f_r = 1$)	—

*Note: Where the main text prints μ8f33 and μ9f34 in equation (S1), the consolidated repair convention of the steady-state system, equations (S69)–(S70), routes the repairs of states 33 and 34 through μ2 and μ6 respectively; see the transcription note in Section S5.

S13. Reproducibility statement and data availability

The complete numerical pipeline of the study is specified in this file to a level sufficient for independent reimplementation. The inputs are the eleven failure and degradation rates and seven repair rates of Table S5, each estimated by maximum likelihood from the screened operational logs under the protocol of Section S2.2; the model is the 34-equation system of Section S5; the transient solver is the RK4 specification of Section S6.1; and the steady-state solver is the Gaussian-elimination specification of Section S6.2 or, equivalently, the closed-form relations (S71)–(S106). The original implementation used Python 3.11 with NumPy 1.26 and the LAPACK dgesv linear-algebra backend; the independent verification of Section S6 used Python 3.12 with NumPy 1.26 and SciPy 1.11 (matrix-exponential propagation for the transient cross-check). Source code and seed values of the original study are available from the corresponding author on reasonable request. The plant operational logs themselves cannot be shared because they contain commercially sensitive production information; the screened event counts (n column of Tables S4 and S5), the monthly aggregates underlying the sensitivity ranges of Section S4, and the bootstrap procedure of Section S8 fully characterise the statistical information used by the model, so all reported figures can be reproduced from the tabulated rates alone, as demonstrated by the verification tables of Section S6.

The following minimal steps reproduce every headline number. First, compute G1, G2, G3 from equations (S101)–(S103) with the baseline rates. Second, compute f1 from the exact normalisation of the recursive relations (S71)–(S100) and obtain $A(\infty)$ from equation (S106); this reproduces Table S6. Third, propagate $f(0) = (1, 0, \ldots, 0)$ through the generator matrix of the transition structure of Table S3 to obtain $R(t)$ at the twelve checkpoints; this reproduces Table S7. Fourth, re-run the steady-state solve for each +10% repair-rate perturbation and convert with T = 8,000 hours and C_d = USD 410; this reproduces Table S9. The entire computation completes in under one second on commodity hardware.

S14. Cross-reference map: Main text to supplementary materials

Table S26 maps every table and figure of the main article to its consolidated counterpart in this file, together with the new verification items prepared for this compilation. Reviewers checking a specific claim of the main text can use this map to locate the underlying data directly.

Table S26. Cross-reference map between the main article and this consolidated supplementary file (new table of this supplementary file).

Main text item	Content	Supplementary item
Table 1	Subsystem inventory and failure modes	Table S1
Table 2	FMEA with risk priority numbers	Table S2
Table 3	Enumeration of the 34 CTMC states	Table S3
Table 4	Anderson–Darling goodness-of-fit results	Table S4
Table 5	Baseline failure and repair rates	Table S5
Table 6	Impact of λ_5 (peeling machine failure rate)	Table S10
Table 7	Impact of λ_7 (hot press failure rate)	Table S11

Continued on next page

Main text item	Content	Supplementary item
Table 8	Impact of λ_{10} (steaming chamber transition rate)	Table S12
Table 9	Impact of λ_{11} (dryer transition rate)	Table S13
Table 10	Impact of μ_5 (peeling machine repair rate)	Table S14
Table 11	Impact of μ_7 (hot press repair rate)	Table S15
Table 12	Impact of μ_2 (steaming chamber repair rate)	Table S16
Table 13	Impact of μ_6 (dryer repair rate)	Table S17
Table 14	Combined λ_1 / λ_5 availability grid	Table S18
Table 15	Combined λ_{10} / λ_{11} availability grid	Table S19
Table 16	Combined μ_1 / μ_5 availability grid	Table S20
Table 17	Combined μ_2 / μ_6 availability grid	Table S21
Table 18	Bootstrap 95% confidence intervals	Table S22
Table 19	Birnbaum importance measures	Table S23
Table 20	Downtime cost under interventions	Table S24
Equations (1)–(36)	Transient state equations, initial conditions, R(t)	Equations (S1)–(S36)
Equations (37)–(70)	Steady-state balance equations	Equations (S37)–(S70)
Equations (71)–(100)	Recursive steady-state solutions	Equations (S71)–(S100)
Equations (101)–(106)	Composite ratios, normalisation, availability	Equations (S101)–(S106)
Equations (107)–(112)	Derivation of G_1, G_2, G_3	Equations (S107)–(S112)
Birnbaum and cost formulas	Importance-measure and cost-model definitions	Equations (S113)–(S121)
Figures 1–7	Plant flow, machine schematics, transition diagram, transient curves	Figures S1–S7
—	Independent verification of G ratios, $A(\infty)$, and cost scenarios	Tables S6, S7, S9 (new)
—	Complete 34-state steady-state distribution	Table S8, Figure S8 (new)
—	Notation glossary	Table S25 (new)
—	Birnbaum importance visualisation	Figure S9 (new)

*Note: “New” items were computed or prepared specifically for this supplementary compilation and do not appear in the main text.